

A STUDY OF HEAVY NUCLEAR TRACKS IN G-5 EMULSION
EMPLOYING PHASE CONTRAST PHOTOMICROGRAPHY

by

ROBERT GARY MCFADDEN

B. S., Case Institute
of Science and Technology, 1959

A MASTER'S THESIS

submitted in partial fulfillment of the

requirements for the degree

MASTER OF SCIENCE

Department of Physics

KANSAS STATE UNIVERSITY
Manhattan, Kansas

1962

TABLE OF CONTENTS

INTRODUCTION AND REVIEW OF LITERATURE	1
Transverse Dimensions of Heavy Nuclei in Electron Sensitive Emulsions.	1
Significance of Charge Determination of Heavy Nuclei	1
Review of Heavy Track Study	2
Characteristics of Tracks of Heavy Nuclei in Electron Sensitive Emulsions	3
Methods of Charge Determination of Heavy Nuclear Tracks in Electron Sensitive Emulsions.	5
The Delta-Ray Method	6
The Thin-Down Length Method.	7
Purpose.	8
PROCEDURE	9
EXPERIMENTAL RESULTS.	20
CONCLUSIONS	32
ACKNOWLEDGMENTS	57
LITERATURE CITED.	58
APPENDICES.	61

INTRODUCTION AND REVIEW OF LITERATURE

Transverse Dimensions of Heavy Nuclei in Electron Sensitive Emulsions

Significance of Charge Determination of Heavy Nuclei. The importance of the width measurements of heavy tracks in electron sensitive emulsions rests chiefly in their utilization in identifying the atomic number Z of the particle causing the track in the emulsion. In the early study of ionographic traces made in emulsions much attention was paid to examining the range, energy, and granularity of track traces. It was not until quite recently that the transverse dimensions of heavy tracks have been accorded the attention of researchers. The problem was formulated in 1948 when the presence of the tracks of heavy cosmic ray nuclei in electron sensitive emulsion stacks, exposed at high altitudes, was first recognized (7). Subsequently, numerous attempts have been made to identify the nuclear species represented by these heavy tracks; these attempts are a consequence of the increasing importance of establishing as accurately as possible the charge distribution of the primary cosmic radiation to comprehend its origin and accelerating mechanism.

Although measurable parameters, which are functions of mass, charge, and velocity, characterizing these heavy nuclear tracks are in common use, the unambiguous identification of the charges of relativistic particles in the range $3 \leq Z \leq 14$ has only recently (1960) proved feasible (18) and at present no accurate method for measuring the charges of heavy non-relativistic particles is available in the literature.

The source of this difficulty lies in the extraction of information from the ionographic traces of these heavy nuclear species; even though, a heavy track contains much more information per unit track length than a light track,

the standard methods of measuring ionization are not feasible for its extraction.

Review of Heavy Track Study. In 1948 Frier et al. (7) observed tracks of heavy nuclei in cosmic radiation. These nuclei were detected by the heavy tracks that they produced in electron sensitive emulsions which had been exposed at high altitudes. Two distinguishable features characterized these heavy tracks: the prolific number of delta-rays projected at all angles from the track, and the thickening and subsequent abrupt tapering near the end of their range. The thickening of the track was attributed to the increased specific energy loss of the bare nucleus as it passed through the emulsion, as predicted by the Bragg ionization curve; and attributed the taper as resulting from the decreased specific energy loss as the effective charge of the nucleus decreased due to electron capture from the emulsion, when the speed of the nucleus reached the range of the speeds of the electrons comprising its inner shells. Pursuing the systematic study of these nuclei, Frier recommended the measurement of the length of thin down as a method of determining the atomic number Z of these heavy tracks.

In 1950 Hoang and Morellet (8) studied some primary heavy nuclei and measured the taper lengths and determined the Z of the nuclei by the classical method called "Method of Delta-Rays". They postulated that the taper length was related to the delta-ray density along the trajectory of the nucleus. However, their experimental taper lengths were not in good agreement with the predicted taper lengths of Frier.

In 1950 Perkins (15) adopted the point of view of Frier, but drew a distinction between "true thinning" explained by Frier and a "pseudo thinning" due to delta-rays of energy greater than 10 Kev.. Accordingly, he stated that this phenomena limited the use of the length of the thin-down to measurements of $Z > 10$.

Cuer and Lonchamp (4), (11), (12) in 1953 suggested a new mechanism of heavy track formation based upon the spatial distribution of the delta-rays ejected by the passage of the primary particle in an attempt at explaining the difficulties besetting Frier's hypothesis. According to these authors the spectrum of the delta-rays explains the variation in thickness as a function of speed, and they rejected the hypothesis of Frier. They also verified the thin-down method of Hoang and Morellet for heavy tracks possessing a charge in the range $Z = 6$ to $Z = 14$. This point of view as to the mechanism of heavy track formation has been progressively ascribed to by other researchers in the field such as Della Corte (1), Evans (6), and by Skjeggested (17), who found experimental values of the track width in the last 150 microns of range in Ilford G-5 emulsion in agreement with Lonchamps' theory for nuclei lighter than oxygen.

In 1961, Gegauff (9) presented a comprehensive study of the structure of the width of heavy tracks in ionographic emulsions, systematizing the various methods of measuring track width and considered the various factors crucially effecting the utilization of each measurement. Further pertinent references may be found there.

Characteristics of Tracks of Heavy Nuclei in Electron Sensitive Emulsions.

The difficulties in applying ionization measurement to heavy tracks stems from the characteristic appearance of these tracks in electron sensitive emulsions. These characteristics are closely related to the parameter Z of the heavy nuclei. Tracks of nuclei of charge $Z > 4$ in electron sensitive emulsions bear the general appearance of a solid core of silver, composed of unresolvable delta-rays that were formed along the trajectory of the nuclear particle by the interaction of the moving particle and the emulsion. Attached to this solid core, and/or in close proximity to it, are a prolific number of delta-rays projecting in all directions.

The trajectory of this core of silver may be subdivided into three general regions that are characterized by the core's width; these are: (a) a high energy region - as the track first enters the emulsion, and for the majority of its trajectory, its core has a narrow width due to the small number of delta-rays of low energy available for the clogging process, associated with the greater velocity of the nucleus; (b) a maximum width region - gradually as the track's residual range decreases as the nucleus approaches the end of its range, where it undergoes a rapid deceleration, more low energy delta-rays are made available for the clogging process, and the core width increases and approaches a maximum; (c) a taper length region - at the extreme end of its residual range, immediately following the maximum of the core's width, the core of the track goes through a pronounced decrease in width due to the rapidly decreasing range and density of the low energy delta-rays, that form the saturated continuum of unresolvable delta-rays that comprise the core of the track, as the nucleus rapidly decelerates. At the extreme end of the residual range, about ten to fifty microns in length depending upon the charge Z , the nucleus begins to capture electrons into bound orbits and thus reduce its effective charge. This process produces a narrow core width at the extreme end of the taper width region, where the track is indistinguishable from that of a proton or an alpha particle. The taper region is usually denoted in the literature as the "thin down" region.

As the parameter Z increases the following track characteristics become more pronounced; (a) the variation in the thickness of the core with respect to residual range becomes more rapid; (b) the increase in the maximum width of the core becomes more pronounced; (c) the thin down at the end of the residual range becomes more emphasized; (d) the prolific number of delta-rays

per unit length of track increases. The distinctive features of the thin-down and the large number of delta-rays per unit length of track that characterize heavy nuclear tracks ($Z > 4$) are in marked contrast with proton and alpha particle tracks in electron sensitive emulsions.

The physical process of the formation of tracks of heavy nuclei in electron sensitive emulsions is explained by Powell et al. (16, pp 172-8), and they depict montages of tracks of various heavy nuclei in the range from $Z = 8$ to $Z = 26$.

Methods of Charge Determination of Heavy Nuclear Tracks in Electron Sensitive Emulsions. The difficulty of utilizing standard methods of ionization measuring to determine the charge parameter of heavy nuclei is evident when viewed in the light of the characteristics of these tracks in an electron sensitive emulsion. The methods of grain and blob counting, although extremely effective in conjunction with their utilization with light tracks, prove ineffectual when applied to heavy tracks due to the large number of unresolvable delta-rays that form a solid uninterrupted core of silver.

The most frequently utilized measurements from which the charge parameter Z may be deduced are the observations of:

1. Residual range.
2. Delta-ray density - the frequency of occurrence per unit length of track of knock on electrons (delta-rays) with energies in excess of a certain minimum value but less than a given maximum value.
3. Track density or diameter of solid silver core.
4. Multiple scattering.

From the first three measurements two different methods of charge determination are possible for electron sensitive emulsions. These methods are:

1. The delta-ray method.

2. The thin-down length method.

The Delta-Ray Method. There exist several methods of charge determination by means of delta-ray counting; however, the one most frequently encountered is the range delta-ray method first employed by Bradt and Peters (4). This method consists in determining the delta-ray spectrum of a particular track by counting the number of delta-rays per unit length of track that have energies between specified limits. The charge parameter Z is then determined by combining this delta-ray count with Mott's (13) relation for the delta-ray spectrum given as

$$n = K (Z^2 / \beta^2) \quad (1)$$

where n is the number of delta-rays per unit of track having energies between W_0 and W_1 , produced in matter having N electrons per unit volume, by an incident particle of charge Ze and velocity β ; and β is a function of the range and the atomic number Z of the incident particle. K is given by the relation

$$K = 2\pi N (e^2/mc^2)^2 (mc^2/W_0 - mc^2/W_1) \quad (2)$$

where W_0 and W_1 are respectively the minimum and maximum delta-ray energies that may be counted.

Normally when performing delta-ray counting techniques, two sets of criteria are employed to determine the values of W_0 and W_1 . These criteria are respectively known as the grain criterion and the range criterion. The grain criterion requires that only those delta-rays possessing a number of grains between a specified maximum and minimum number may be counted; where as, the range criterion requires that only those delta-rays possessing horizontal ranges perpendicular to the track's trajectory between a specified maximum and

minimum range may be counted. The values of W_0 and W_1 are obtained for the imposed grain and range limits respectively from the grain number-energy curves and the range-energy curves for electrons.

The Thin-Down Length Method. Upon entering the atmosphere a heavy nucleus is stripped of its orbital electrons and remains in that state as long as its speed is greater than the speed of its inner shell electrons. Originally, the thin-down length method as proposed by Frier et al. (7), assumed that the thin down process of a heavy nuclear track in an electron sensitive emulsion starts as the nucleus' speed reaches the range of values of the speeds of its inner shell electrons. For at such speeds, the incident nucleus becomes capable of capturing electrons from the emulsion; hence, diminishing the track diameter as the effective charge that it possesses approaches zero. The length of this thin down ("true thin-down") may be correlated with the parameter Z . However, the true thin-down length is not the thin down length observed in electron sensitive emulsions; rather, a "pseudo thin-down" length is observed. The explanation of this pseudo thin-down is based upon the fact that a saturation of delta-rays of low energies comprise the central core of the track. Pseudo thin-down begins at the range where this saturation of delta-rays starts to decrease. This measurable pseudo thin-down length may be correlated with the parameter Z in a relation of the form

$$L = a Z^{\kappa} \quad (3)$$

where the values of a and κ have been experimentally determined by Hoang and Morellet (8); whose work has been theoretically confirmed by Lonchamp (11) for $Z = 6$ to $Z = 14$.

Although delta-ray counting provides a useful technique for the studying of heavy tracks, it often proves difficult to decide whether a particular

collection of grains constitutes a delta-ray with the result that the delta-ray density is a subjective parameter, not readily reproducible when the heaviest tracks are under consideration. Similarly, the measurement of track width is a subjective, hard to reproduce, parameter when heavy tracks are under consideration, since it proves difficult to determine what constitutes a measure of track "width" when the central core of the track is immersed in a prolific number of heavy delta-rays. Multiple scattering measurements also yield subjective parameters in that the actual trajectory of the nuclear particle is difficult to perceive among the gross variations in direction caused by the attached delta-ray clumps.

Parnell (14) gives references to the delta-ray counting techniques employed by various workers in this field through 1951 and presents a review of the thin-down method. Further references covering the time interval between 1951 and 1962 may be found in Evans and Hillier (6) and especially in Gegauff (9).

Purpose

According to Gegauff (9), four methods exist for the determination of the track widths of heavy nuclei in electron sensitive emulsions, they are:

1. Filar micrometer.
2. Micrometer with parallel faces, sold under the trade name "Pochstrolino".
3. Photometry.
4. Microphotography.

The research embodied in this paper has dealt with the photographic aspect of the problem of determining the width of heavy nuclei in electron sensitive emulsions.

In 1961 E. Obi and the writer observed a phenomenon under a phase contrast microscope equipped with a Heine condenser while employing this microscope in the examination of tracks in a stack of Ilford G-5 stripped emulsion. By appropriate settings of the phase condenser, the background and the granularity of the emulsion could be made to disappear, leaving only the trajectories of the very thick nuclei, stripped of the majority of their loose associations of delta-ray clumps, in the field of view. This phenomenon seemed to present a method of optically eliminating the two factors that cause the parameters of track width and delta-ray density to be subjective; they are: (a) the loose associations of delta-rays that lie in close proximity to the track, and (b) the confusing granularities of the emulsion in the vicinity of heavy tracks. The present investigation was conducted with the view to developing this optical phenomenon into a systematic optical method of obtaining duplicable track width measurements of heavy nuclei, in order to employ these track width parameters in the calculation of the atomic charge Z of the investigated nuclear species.

PROCEDURE

All track parameter measurements presented in this paper were performed upon a heavy nuclear track designated 17_{a4} in a stack of five Ilford G-5 pellicles each of which was nominally 5 x 10 cm x 1000 microns thick. This track was traced photographically through two pellicles to the point where it entered the stack. Charge and width determinations had been made previously upon this track by Parnell (14) and by Cline (3), where additional references to the particular stack of pellicles used may be found. Parnell employs the designation of track 17_{a4} used in this paper, while Cline refers to this track as track 1. The two pellicles through which track 17_{a4} was traced bear the

following designations; (a) 18_a is the pellicle where the track enters the stack, (b) 17_a is the pellicle in which the track was stopped and contains the taper and maximum width regions as well as part of the high energy region.

All photographic measurements were taken with a Leitz Aristophot used in conjunction with a Leitz Ortholux microscope. The Leitz Aristophot was equipped with a bellows camera to which a polaroid land camera back was attached. The Leitz Ortholux microscope employed a 20X phase contrast objective (catalogue number PHANC₁) in conjunction with a Heine condenser.

The montages of track 17_{a4} depicted in Plates IX through XXIX were taken upon polaroid transparencies, type number 46L, with a bellows extension of 57 centimeters utilizing a 10X Leitz photographic eyepiece (catalogue number PEZEN) and a carbon arc light source. The backgrounds of the individual photographs were then matched and the range of appropriate points marked. These matched photographs were then cut and fitted into three separate montages upon a continuous roll of matted drafting acetate. From this mounted roll of montages contrast prints were made.

The three montages depicted in Plates IX through XXIX are of the same nuclear track, 17_{a4} , but each was taken employing a different setting of the Heine condenser, to be designated as α , β , γ . The α , β , γ -montages correspond respectively to figures 1, 2, and 3 of Plate IX. The α -montage was taken in bright field illumination, while the γ -montage was taken with the image of the annular light source centered directly in the center of the annular phase ring as viewed in the Leitz focus magnifier (catalogue number PHADS). The β -montage was obtained by centering the image of the annular light source upon the inner edge of the annular phase ring; this was accomplished by advancing the image of the annular light source just into the phase ring and then backing it slowly out until the image of the annular

light source brightens. When the β -position is properly set upon the Heine condenser the background illumination of the field of view in the eyepiece (10X - Leitz catalogue No. PERIR) of the microscope possesses a characteristic golden hue and the taper regions of heavy tracks will be outlined by a gold edge¹. Note that the microscope must first be focused before the β , or δ settings are made. Also, note that the width differences as a function of the residual range is very pronounced between the different montages; the width of the β -montage is always smaller than the width of the α -montage, as a function of residual range.

Residual range determinations were first made by photographing a stage micrometer scale to obtain the magnification factor. Utilizing this magnification factor (microns/millimeter), the projected residual range was then directly marked off on the film in microns. This measurement of projected residual range was checked against that obtained by using the Leitz precision stage micrometers, where projected residual range was given by

$$R_p = \left\{ (\Delta x)^2 + (\Delta y)^2 \right\}^{1/2} \quad (4)$$

where Δx and Δy were the horizontal distances from the end of the track, in microns. The stage micrometer range values were checked by measuring the end points of the track in the 17_a pellicle and comparing this range against the value obtained by segmenting the track in the 17_a pellicle and measuring the length of each of these segments and then adding these lengths to give a projected range figure for the whole length of the track in the 17_a pellicle. These two values agreed to within 1 part in 3500. Then the values of the range points of conspicuous features, such as light tracks crossing the heavy track, of the heavy track 17_{a4} as found by direct scale measurement and by stage micrometer measurement were plotted against each other to yield a weighting

¹ phenomena associated with use of a Leitz green filter.

function to bring the scale measured projected range points into agreement with the stage micrometer values. When this was accomplished, the projected range points agreed to within 1% of the stage micrometer values. The actual residual range was obtained from the dip angle of the track and the weighted projected range via the formula

$$R = \frac{R_p}{\cos \theta} \quad (5)$$

where R is the true residual range and R_p is the projected range. θ is the dip angle of the track and was determined from the formula

$$\tan \theta = \frac{\Delta z S^n}{\bar{R}_p} \quad (6)$$

where Δz is the vertical distance from the end of the track to where it left the pellicle in microns, S is the shrinkage factor, n is the index of refraction, and \bar{R}_p is the projected range of the track from the end of the track to where it leaves the pellicle. (For Ilford G-5 emulsions $S = 2.7$, and $n = 1.50$). Note that the three montages represented in Plates VIII through XXVI are matched with respect to each other in terms of the residual range and the true residual range scale on the α -montage holds also for the β and γ -montages.

The track width was obtained by projecting portions of the β -montage on to graph paper and tracing their outlines by hand; after which planimeter measurements of the tracings were performed over small given intervals (approximately 60 microns in length) chosen at random along the length of the track to obtain an average track width over such intervals. Only the core of the track was traced; the thick delta-rays that were attached to the core that the condenser setting could not completely cause to disappear were arbitrarily chopped through at their base - the error in the planimeter measurements caused by this arbitrary chopping through of the area of the base of

these delta-rays cause a fluctuation in thickness that is well under a tenth of a micron.

Grain diameter as a function of depth was determined for the complete depth of pellicle of 17a by following a moderately high dip angle track, using a 100X Leitz KS oil emmersion objective, through the emulsion and at various depths measuring the grain diameter, with a 12.5X Leitz micrometer eyepiece, of every third grain as well as measuring their depths. Ten grains were measured at each depth. From this data an average depth versus an average grain diameter was computed throughout the 17a pellicle. In a similar fashion the grain diameter as a function of depth was determined for a portion of the 18a pellicle near its junction with the 17a pellicle. The standard deviations in the average depth covered so small a range that when graphs of grain diameter versus depth and grain diameter versus residual range were plotted they could not be depicted. Plate I portrays the relationship between grain diameter and depth of pellicle for pellicles 17a and 18a. From this relationship the grain diameter versus residual range plot depicted in Figure 2 of Plate 3 was computed with the aid of relation (5).

In using the track width parameter to calculate Z a question might arise as to just what this width means, since the width shrinkage due to the use of phase optics apparently varies with the thickness of the track. To escape such difficulties a method was devised that depended only upon knowing the range at which the maximum thickness occurred, and such a point may be determined from the track width versus residual range plot of Figure 1 of Plate IV, without going into detail about the mechanism of the diminishing of the track width by the optical process of the phase contrast microscope.

EXPLANATION OF PLATE I

Relationship between grain diameter of Ilford G-5 Emulsion versus the depth in the emulsion for pellicles 17a and 18a.

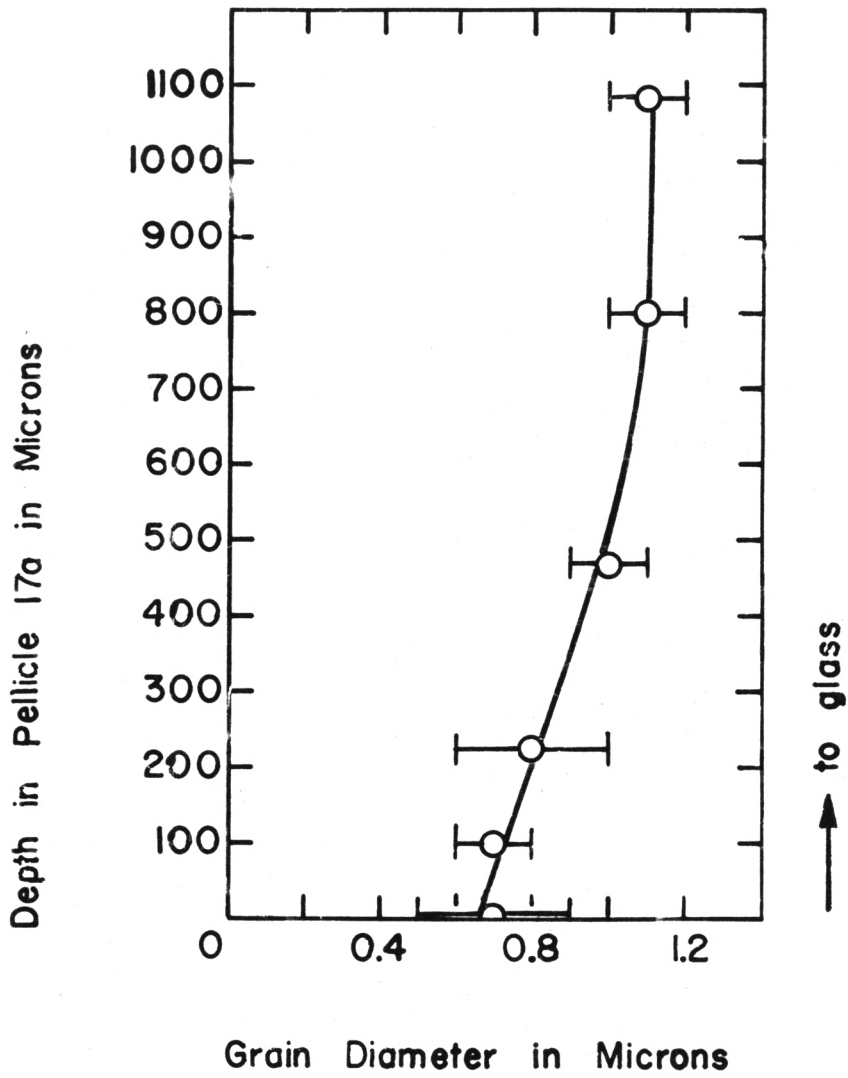
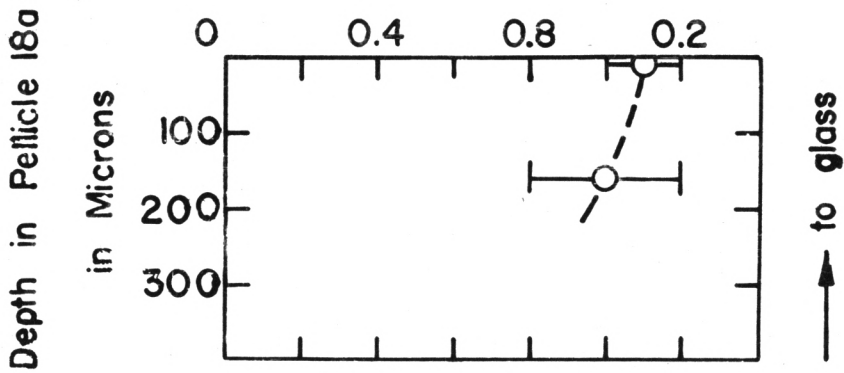


PLATE I



This method consists in considering equation (1) that describes the delta-ray density.

$$n = \frac{2\pi N Z^2}{\beta^2} \left(\frac{e^2}{mc^2} \right)^2 \left(\frac{mc^2}{W_0} - \frac{mc^2}{W_1} \right) \quad (1)$$

Following Lonchamp (12), it is noted that a track will display an opaque core out to the range of a delta-ray of energy W_0 if there are 400 delta-rays per 100 microns of track length having energy between W_0 and the maximum energy $W_1 = 2m_e c^2 \beta^2$ which an electron can acquire in collision with a heavy ion moving with velocity β . When this consideration is incorporated into equation (1) and solved for W_0 we obtain via Katz and Parnell (10), and Skjeggstad (17)

$$W_0 = \left[\frac{1020}{1.5 \times 10^5 \beta^2 / Z^2} + \frac{1}{\beta^2} \right] \quad (7)$$

Thus, W_0 is directly related to the width of the track in a one to one fashion since the distance R from the path of the primary particles to which an electron possessing energy W_0 can travel may be approximated by the relation

$$R = a W_0^{1/2} \quad (8)$$

valid for an electron of low energy (16); hence, the residual range at which W_0 goes through a maximum for a particular value of Z must be the residual range at which the thickness of a nuclear track of that value of Z goes through a maximum. Using Demers' (5) residual range-energy curves for various heavy nuclei of differing values of Z in conjunction with the energy-velocity relation (A = atomic No. of primary particle)

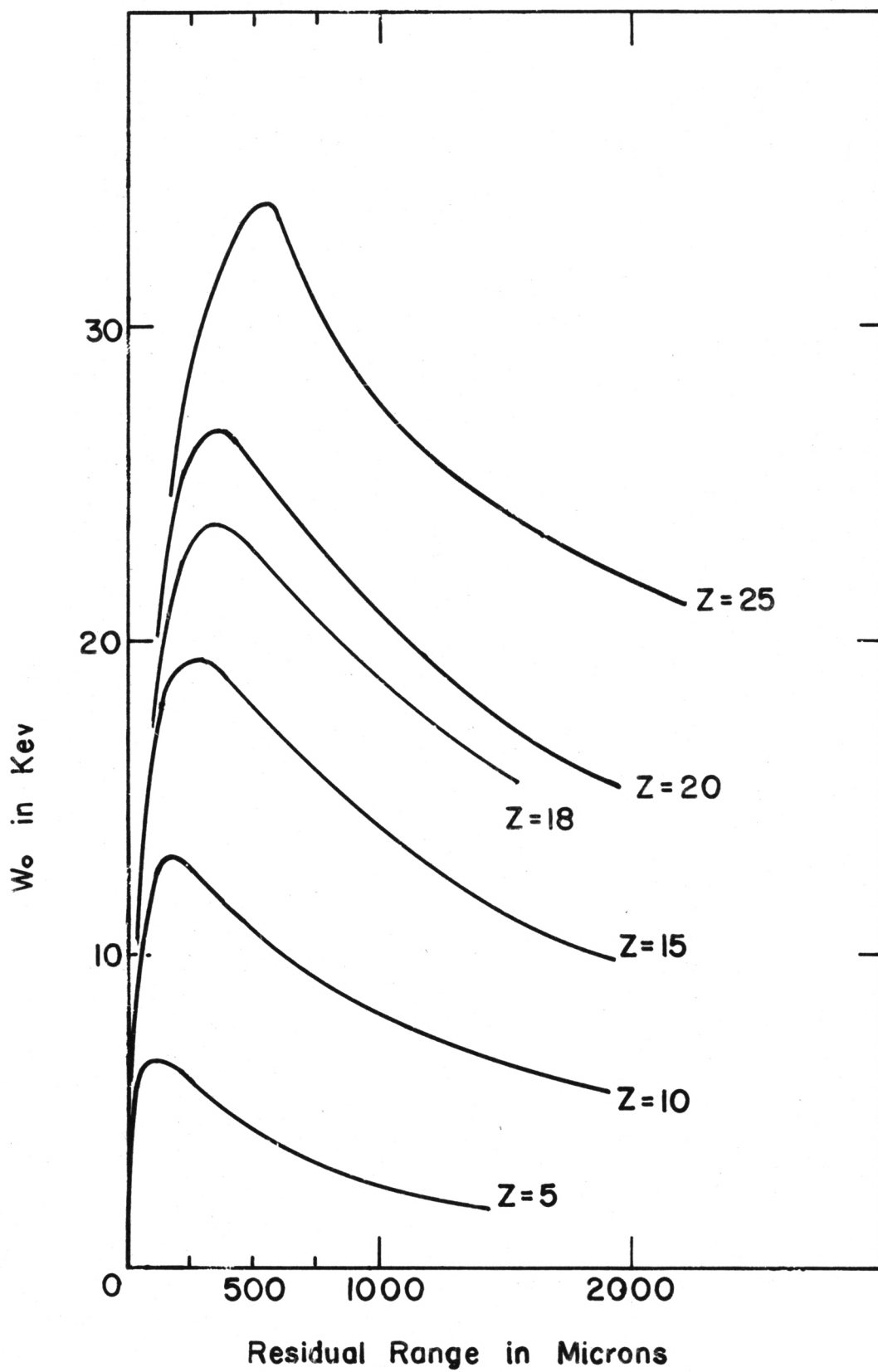
$$E = 1/2 A (931) \beta^2 \quad (\text{Mer}) \quad (9)$$

the residual range as a function of velocity for various values of Z was computed. From this range - velocity relation and relation (7) W_0 as a function of residual range for various values of Z were computed and plotted in Plate II. Employing the curve of Plate II, a curve of atomic change versus the range at which maximum track width occurs was constructed and plotted in Plate VII. Utilizing the residual range value at which the maximum of the locus of the experimental track width versus residual range (displayed in figure 1, Plate IV) occurred, the charge of track 17a4 was determined.

EXPLANATION OF PLATE II

Theoretical plot of W_0 (the energy of a delta-ray which possesses a range equal to the opaque core width of the track) versus residual range for values of $Z = 5, 10, 15, 18, 20,$ and 25 .

PLATE II



EXPERIMENTAL RESULTS

Examination of the three montages depicted in Plates XIII through XXVI, indicating that appreciable variations in thickness exist between them at the same residual ranges. The outlines of the track are much sharper for the β -montage; in fact, the β -montage appears as if the outline of the solid core could be easily traced out - this is not true of the appearance of the α -montage; the outline of its core is very rough and ill defined.


The non-feasibility of performing planimeter measurements upon the α -montage (bright field illumination) was aptly demonstrated by Cline (3). A copy of Cline's Plate VIII illustrating the planimeter determinations of the track width that he performed upon track 17a4 while employing bright field illumination is shown in Plate III. It is evident from this plate that no useful measure of the track width parameter is likely to be obtained employing bright field illumination.


In the course of investigating the width parameter of track 17a4, filar and photometric measurements were performed. It was observed as Gegauff (9) noted, that filar micrometer measurements are useless as a means of determining width measurements of a heavy track. Photometric measurement performed upon a Leeds and Northrop photometer proved as equally dissatisfying as the filar determinations.

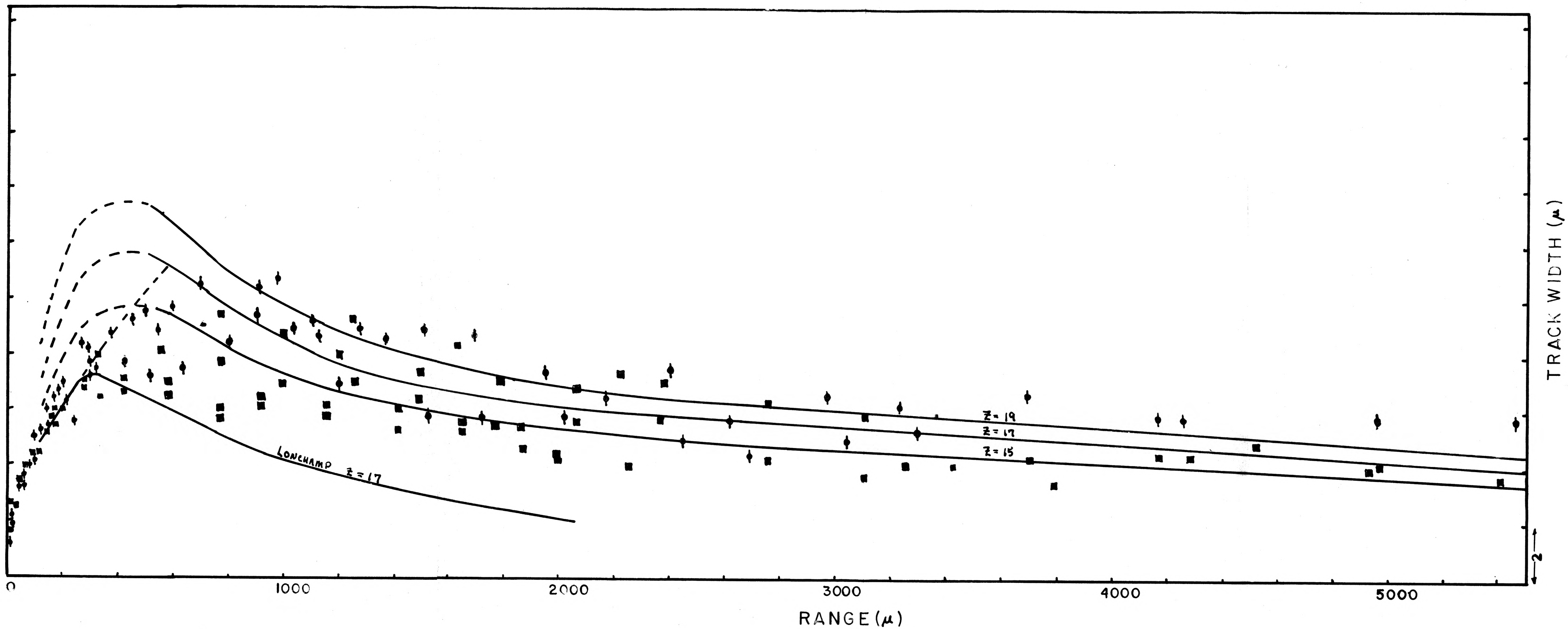
On the basis of Cline's planimeter measurements in bright field illumination; the unsatisfactory data yielded by filar and photometer data; and the clear cut appearance of the β -montage, all planimeter measurements were performed upon the β -montage, in an attempt to determine a track width parameter. Due to the lack of contrast the γ -montage was discarded as being useless for the extraction of track width data.

EXPLANATION OF PLATE III

Plot of Cline's experimentally derived width data for track 17a4.

Visual measurements of track width are denoted by symbol  .

Photomicrographic measurements of track width are denoted by symbol  .



The results of the extraction of track width data from the β -montage is shown in figure 1 of Plate IV. Upon comparing this figure with the results of Cline, depicted in Plate III, the use of the β -montage to extract a track width parameter was a decided success; note that the thin down region is concisely fixed by only six points in the β -montage, while Cline's thin down region needs at least two to three times this number to determine its outline. Also, note that the statistical deviations of track width in figure 1 are generally within 10% and tend to form a well defined locus, while the taper appears much steeper than those obtained for nuclei possessing a Z less than or equal to that of oxygen (17). Other interesting features of the graph depicted figure 1 present themselves. It is noted that as the nuclear track enters pellicle 17a from 18a, that its width abruptly goes through a discontinuous decrease. The question presents itself as to why it should behave in this fashion. The energy and velocity of the particle are nearly the same on either side of the pellicle junction and the track is in the high energy region, therefore, the cause must lie in the emulsion.

Examining figure 2 of Plate IV reveals that the grain diameter stays relatively constant over the thin down and maximum width region of track 17a4; but that it gradually undergoes a continuous degradation in size, with a slowly varying gradient, as the residual range decreases until it crosses the pellicle. In crossing the pellicle junction into pellicle 18a, the grain width undergoes an abrupt discontinuous jump back to the former level that it occupied in the thin down and maximum width region of the track in pellicle 17a. This behavior of the grain width with residual range can only be explained upon the basis that the emulsions of the pellicles were assymmetrically processed by mounting them on plates with one side of the emulsion mounted against the glass and the other side exposed to air.

EXPLANATION OF PLATE IV

Track width and grain diameter data as a function of residual range.

Fig. 1. Track width in microns as a function of residual range of track 17a4 in microns.

Fig. 2. Grain diameter in microns as a function of residual range of track 17a4 in microns.

Grain Diameter in Microns

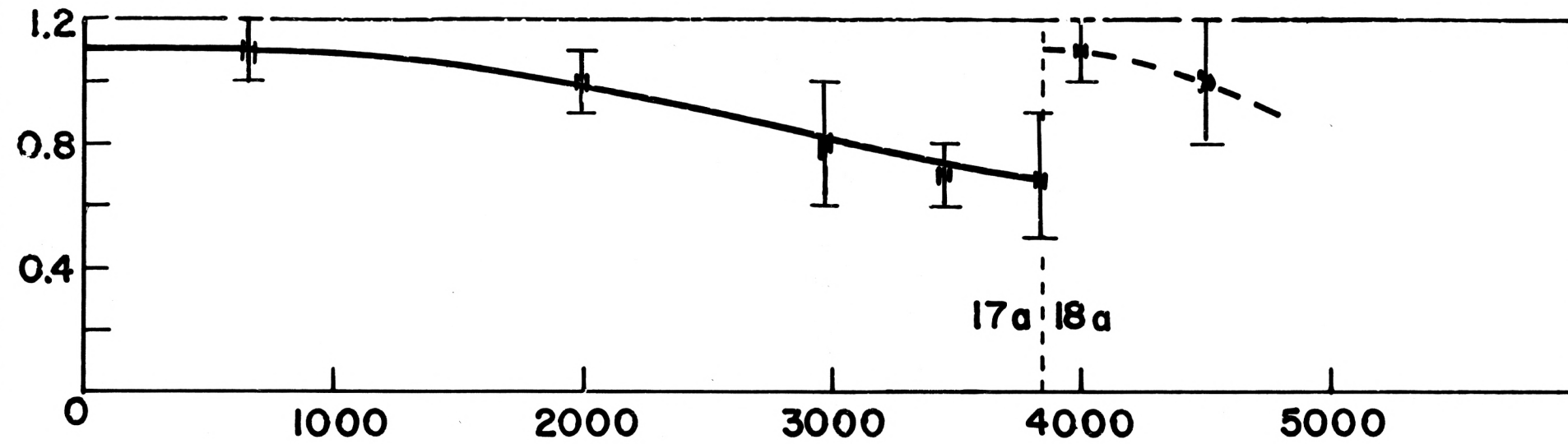
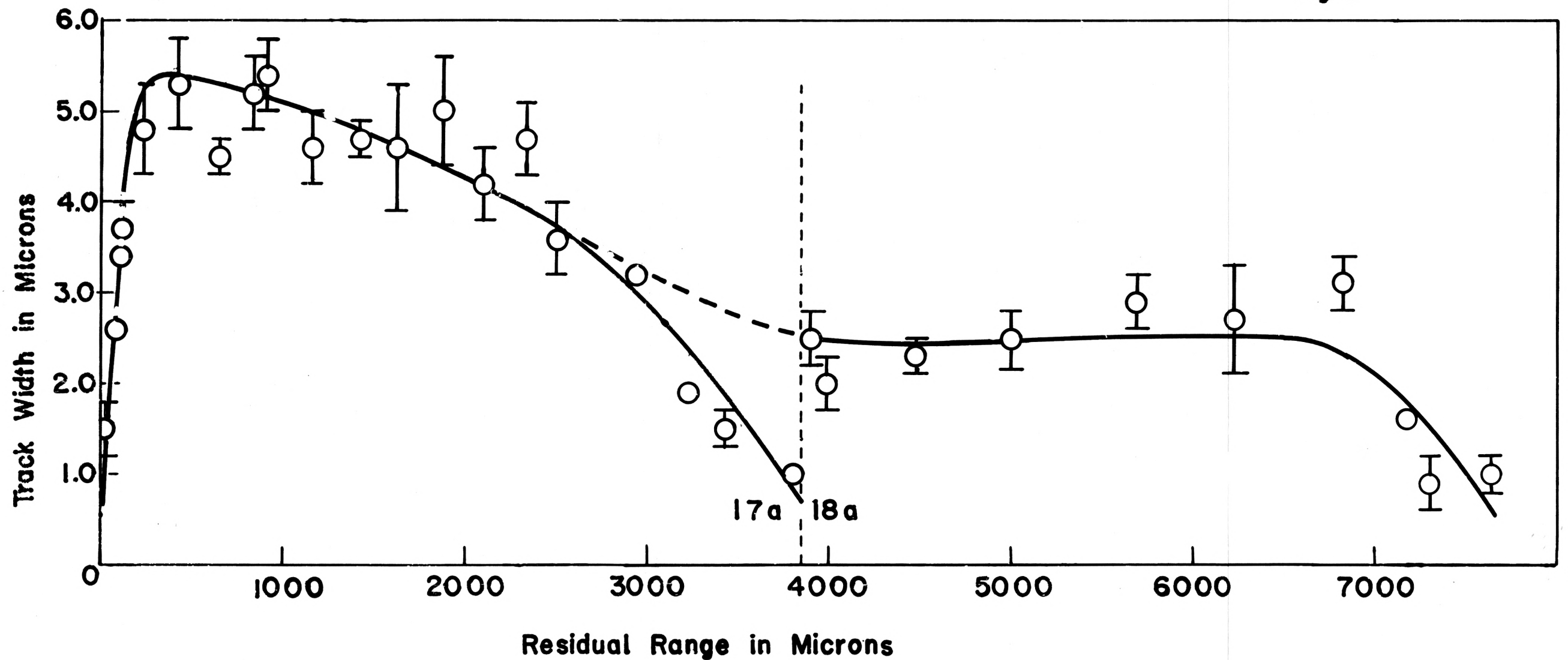


Fig. 2

PLATE IV

Fig. 1



Residual Range in Microns

When these pellicles were processed non-uniform bleaching of the grains took place during the time they were exposed to the reducing agent; the side exposed to air receiving the full action of the reducing agent while the side mounted against glass would have received the action of only the small amount of reducing agent that was able to diffuse to it during the processing period. Hence, a continuous gradient will exist in the grain diameter as a function of residual range or depth in the pellicle.

The question now arises as to how the gradient in grain diameter can effect the width of the track. Since the abscissa of figure 1 and figure 2 of Plate IV are identical, the ordinates of each graph at each common abscissa point in the high energy range were plotted against each other. This yielded the graph of track width versus grain diameter in Plate V. We note that the points on this graph fall along a straight line having a steep positive slope. Hence, a correlation exists between the grain diameter and the track width; that is, the grain diameter is lineally related to the track width. Thus the graph provides the explanation of the behavior of the track width in the high energy region of pellicle 17a that is depicted in figure 2 of Plate IV.

Plate VI depicts the duplicability of the track width measurements of Figure 1 of Plate III. These measurements were made independently of those of figure 1 and have been superimposed upon the locus of the graph drawn in figure 1. The majority of these points in Plate V exhibit a variation in width of less than 10 per cent and fall in the same general regions as the points plotted in figure 1. This would imply that this method of determining the track width parameter is duplicable.

Plate VII depicts the theoretical graph of the residual range at which a heavy nuclear track has its maximum width versus the charge Z it possesses.

EXPLANATION OF PLATE V

Relation of track width in microns versus grain diameter in pellicle
17a in microns.

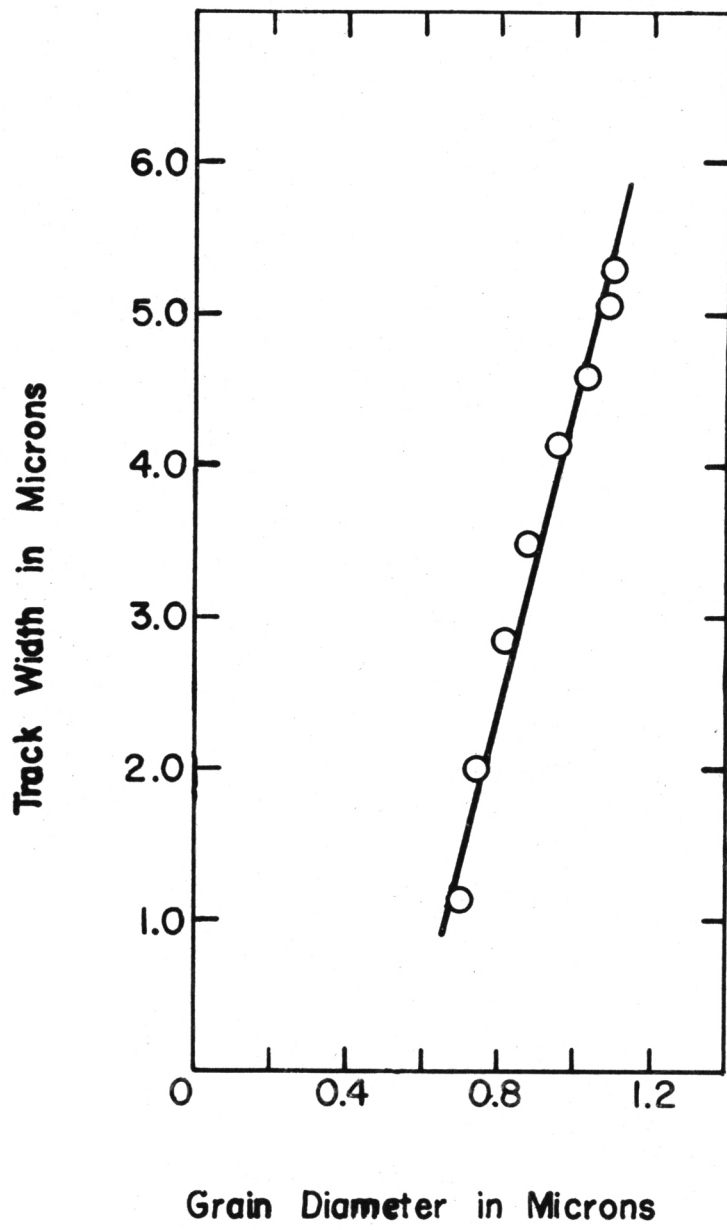


PLATE V

Employing the data of figure 1, Plate IV, this graph yields a charge determination of the nuclear particle moving through the emulsion and this charge was determined as $Z = 18$; therefore, from the appearance of these graphs, the track is that of an Argon nucleus. Cline determined the value of the charge of this track as $Z = 17 \pm 1$, while Parnell arrived at a charge of between 29 and 32 for track 17a4 from delta-ray density and taper measurements. However, the comparison of photographs of this track with published photographs (16) shows agreement with Cline's estimate.

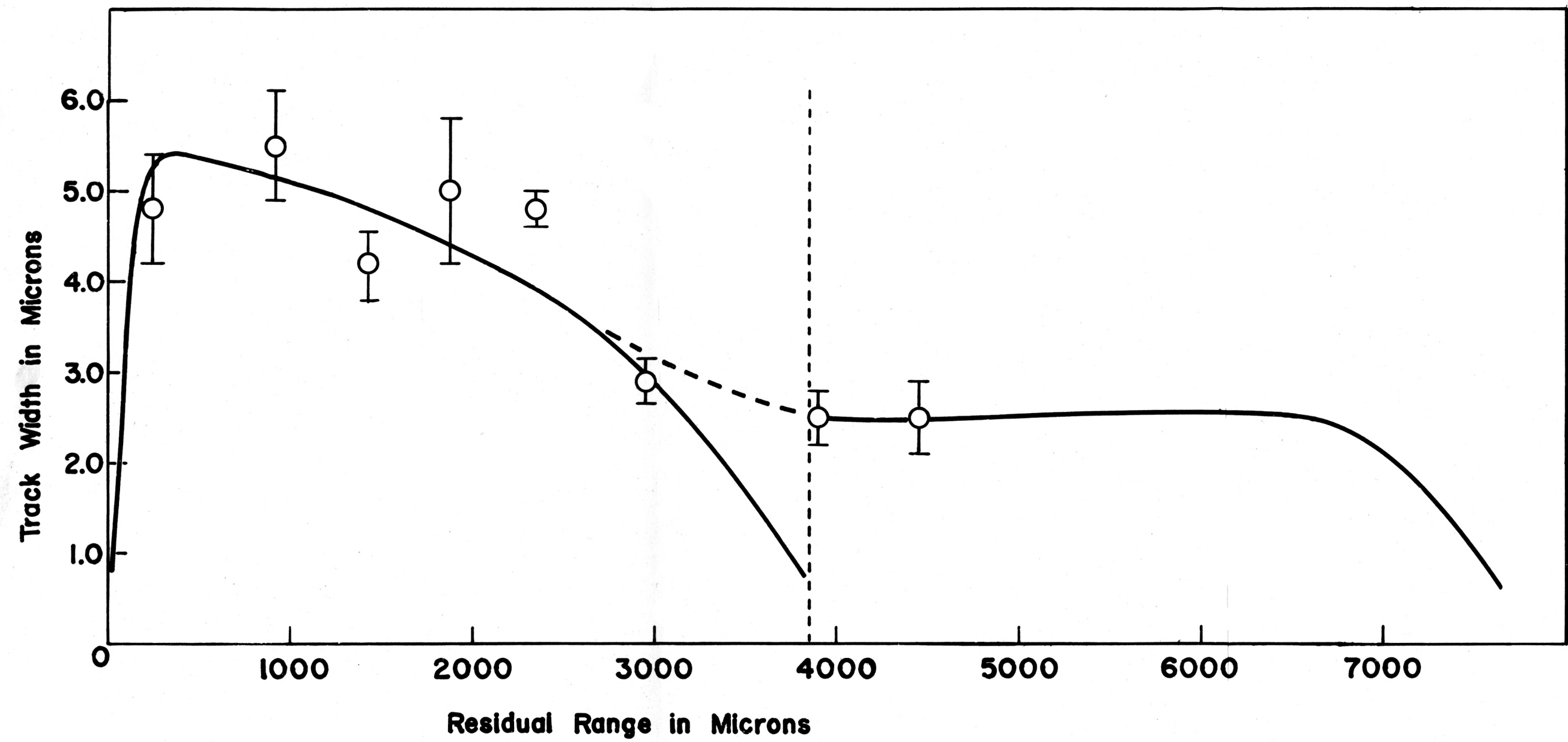
Applying the method of Hoang and Morellet, as described by Parnell (14), yields a charge between 32 and 35 and a plot of the squares of the diameters of the widths of taper lengths of this track lies upon a straight line going through the origin as they predict. However, this method of charge determination rests upon the ratio of the diameter of the track just before thin-down to the diameter of the track near the end of it. But, measurements made upon the widths of the various quartz-fibres shown in Plate VIII, indicate that the width of a quartz-fibre viewed in the β -mode of illumination is less than the width it has when viewed under bright field illumination. Also, the amount of width disappeared varies as the width of the quartz-fibre is changed. This implies that the track width parameter measured in the β -mode of illumination must be function of the actual width of the track; invalidating the use of the Hoang and Morellet thin down method until the functional dependence of the width parameter under the β -mode and the true width of the track is known. This has not been explored further in the present work.

In that an optimum optical illumination arrangement employing the carbon arc as the light source was impossible to achieve, the control of film contrast and exposure time (these quantities are essential to good planimeter traces) proved almost impossible.

EXPLANATION OF PLATE VI

Duplicability of track width measurements as a function of residual range. The solid locus over which the data is superimposed is that of figure 1, Plate IV.

Plate VI



However, the recent employment of a Xenon light source has solved this problem; and photographs of consistent quality may be repeatedly obtained.

The appendices contain short articles dealing with the geometrical optics of the microscope with respect to its use with bright field or with phase illumination.

CONCLUSIONS

A feasible method of measuring non-subjective track width parameters by the use of phase contrast techniques has been delineated, and this parameter may be used to compute values of the charge of heavy nuclei. However, to confirm these conclusions, my results must be duplicated with regards to track width parameter measurements by an independent observer and my determination of charge must be verified from the methods of multiple scattering theory, to which the β -condition will handily lend itself.

EXPLANATION OF PLATE VII

Theoretical graph of the residual range at which a nuclear track has its maximum width versus the charge Z it possesses.

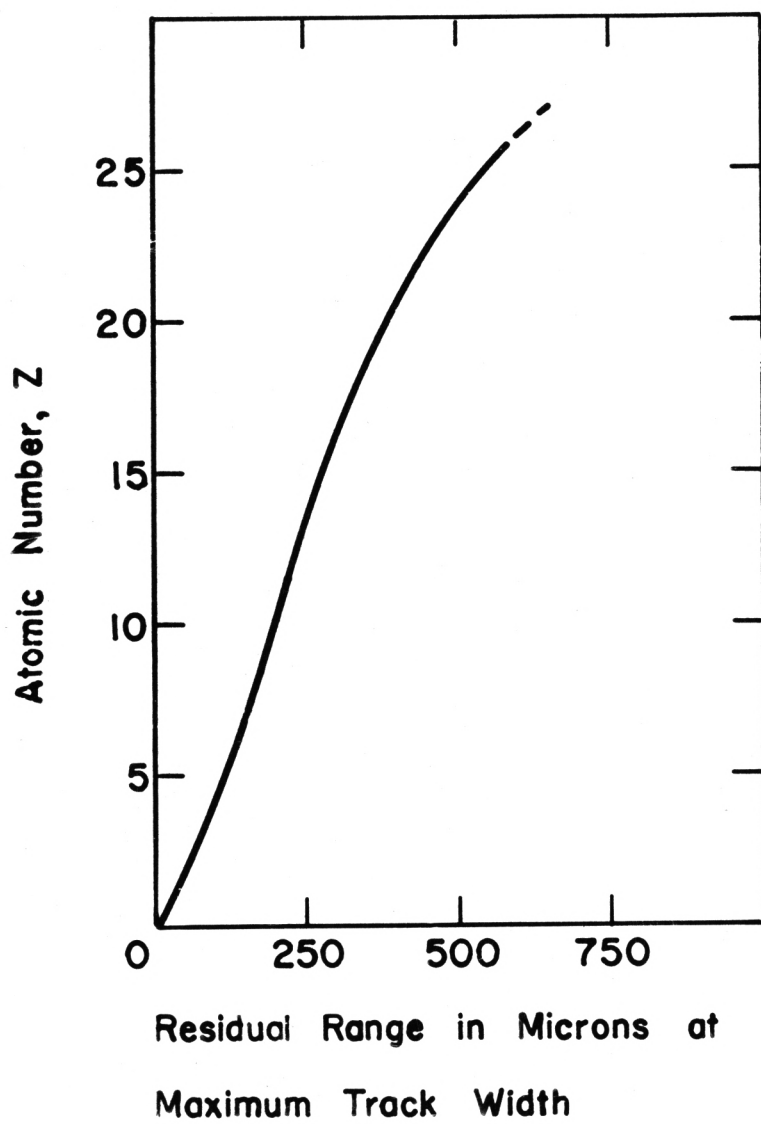


PLATE VII

EXPLANATION OF PLATE VIII

Photographes of quartz-fibres taken under bright field and two modes of phase contrast illumination.

Fig. 1. (a) Thick quartz-fibre taken in α -position (bright field)

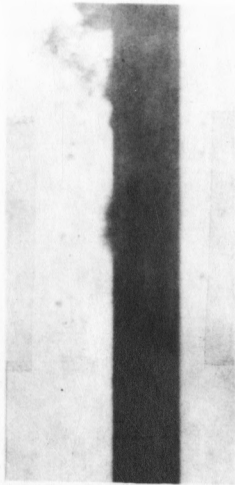
(b) Thick quartz-fibre taken in β -position

(c) Thick quartz-fibre taken in γ -position

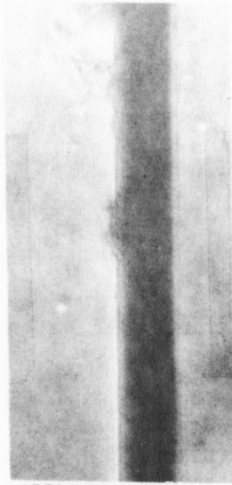
Fig. 2. (a) Thin quartz-fibre taken in α -position (bright field)

(b) Thin quartz-fibre taken in β -position

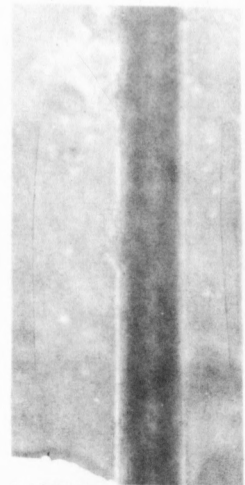
(c) Thin quartz-fibre taken in δ -position



L158103



L158103

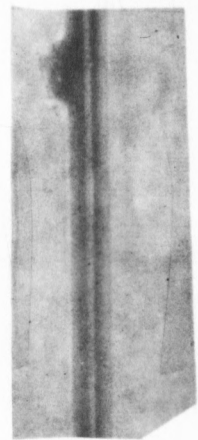
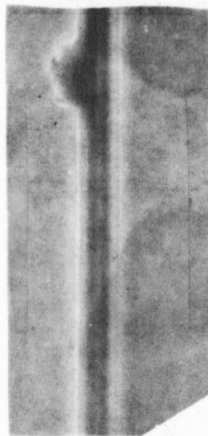
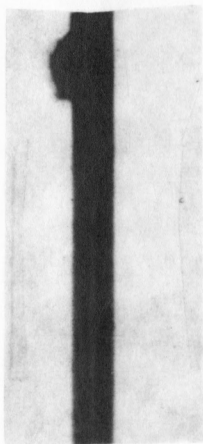


L158103

Figure-2a

Figure-2b

Figure-2c



EXPLANATION OF PLATE IX

Photographs of track 17a4 taken in bright field and two modes of phase contrast illumination.

Fig. 1. Track 17a4 taken in α -position
(bright field illumination)

Fig. 2. Track 17a4 taken in β -position

Fig. 3. Track 17a4 taken in γ -position

(Residual range is given in microns and is plotted against the track of figure 1. This range scale holds for figure 2 and figure 3. Figure 1, 2, and 3 are arranged in a one to one correspondence.)

PLATE IX

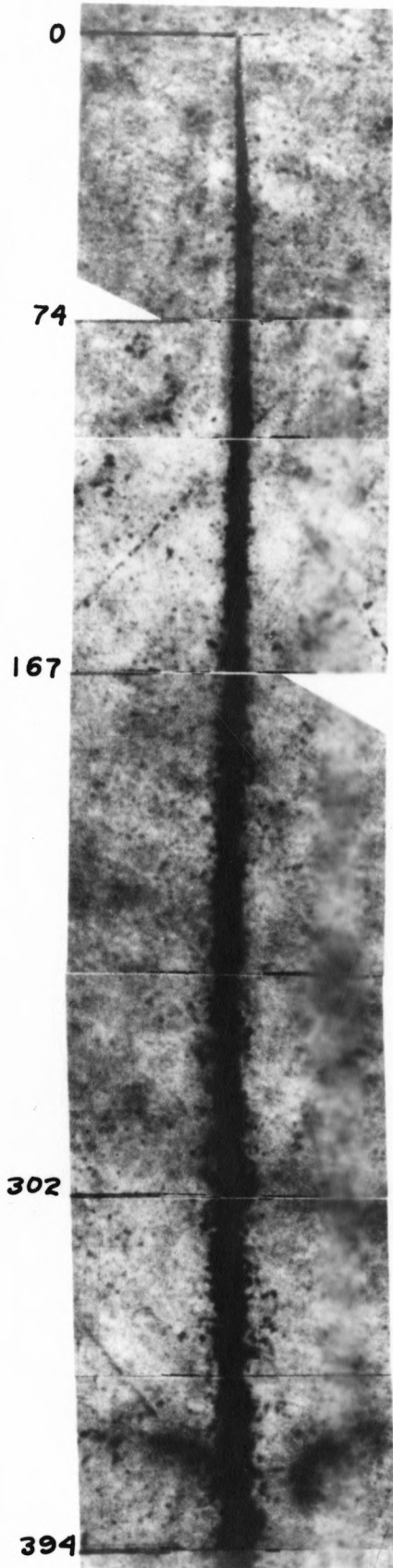


Fig. 1

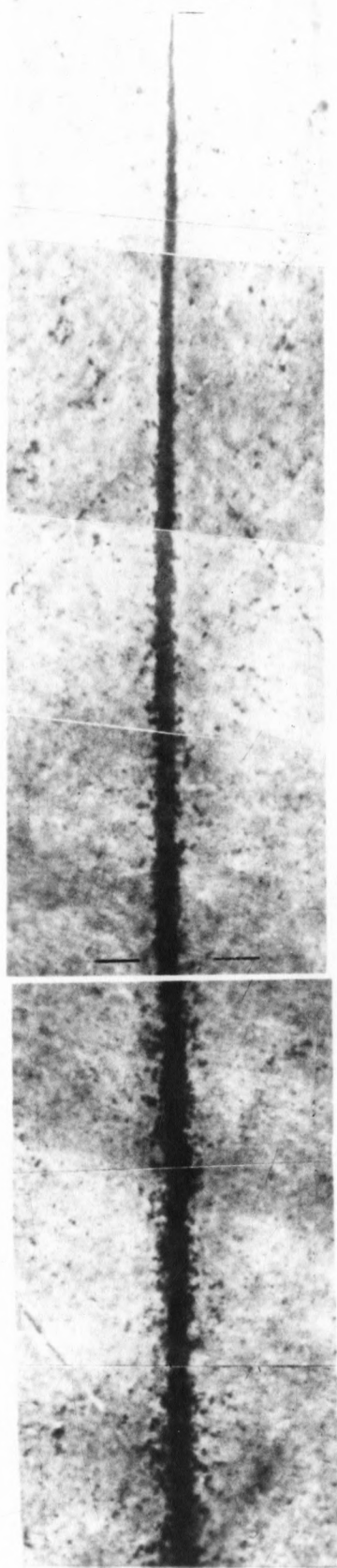


Fig. 2

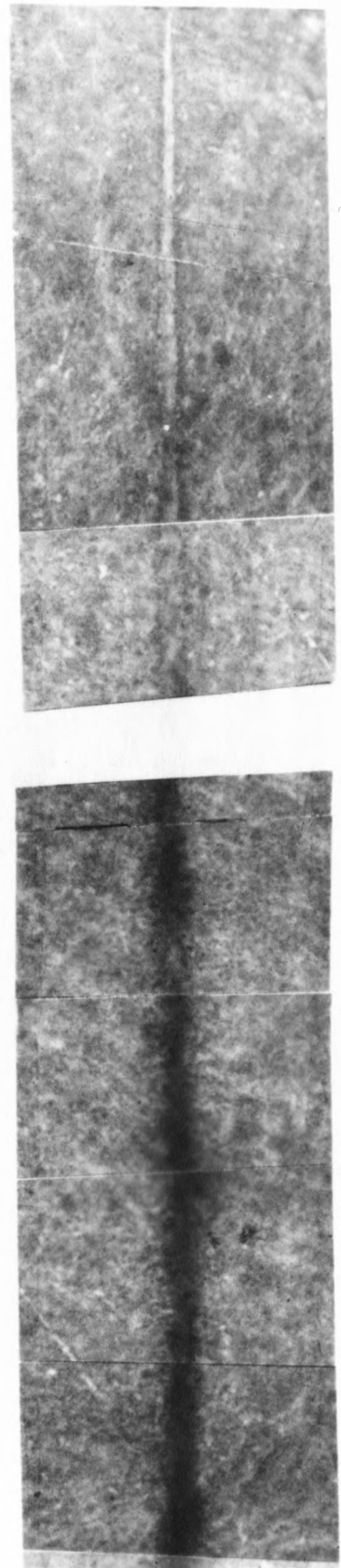


Fig. 3

EXPLANATION OF PLATES X TO XXIX

Continuation of track 17a4

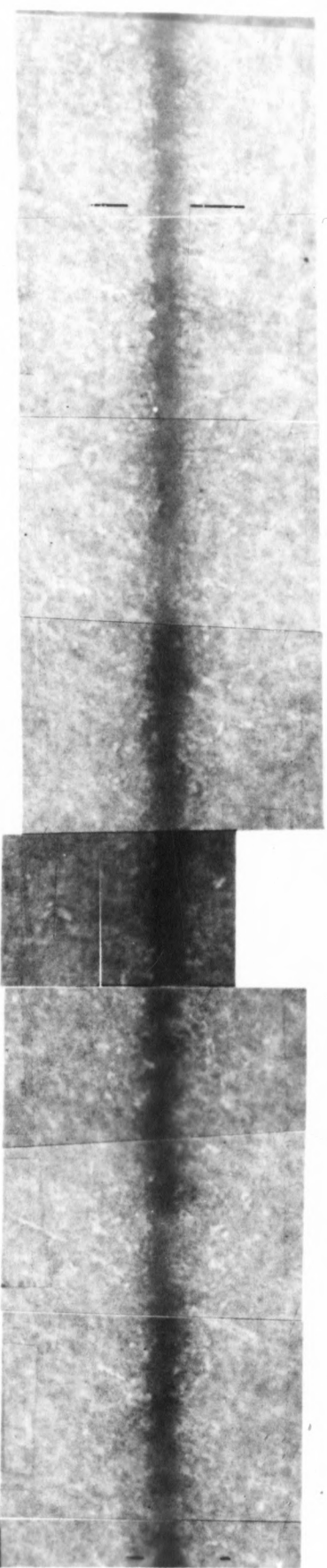
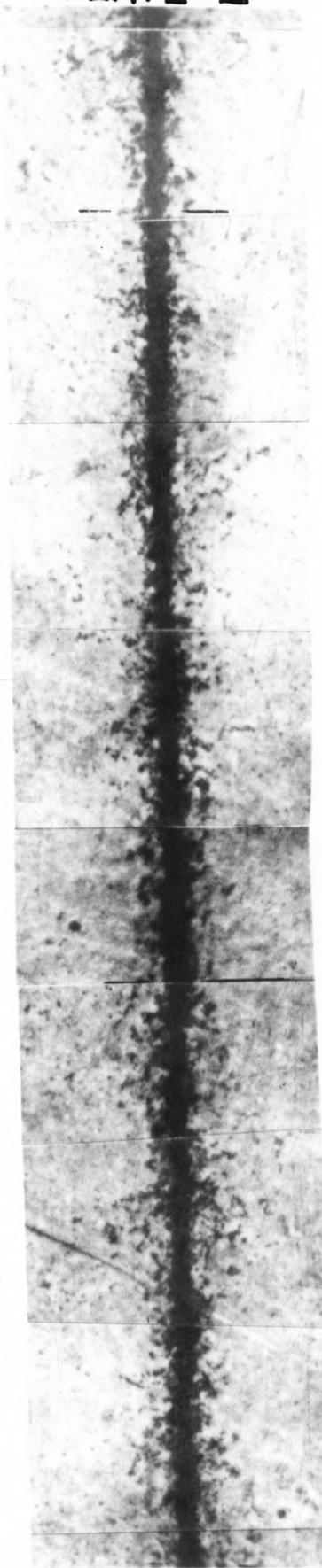
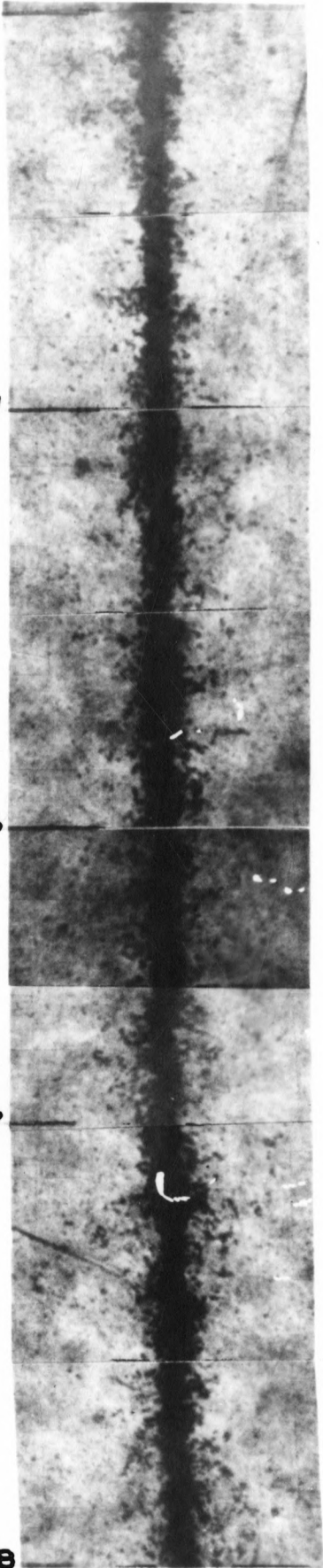
PLATE X

501

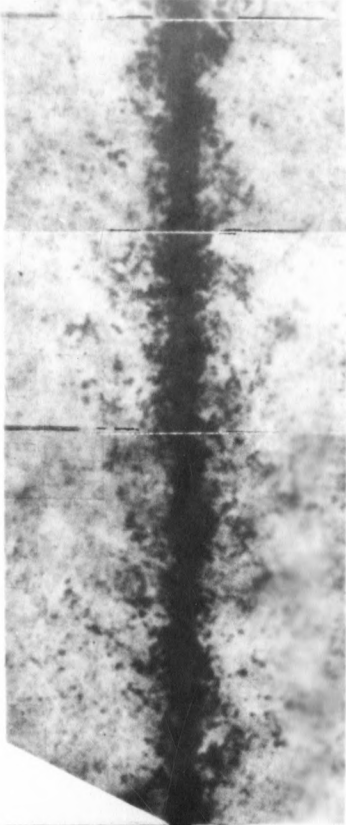
616

697

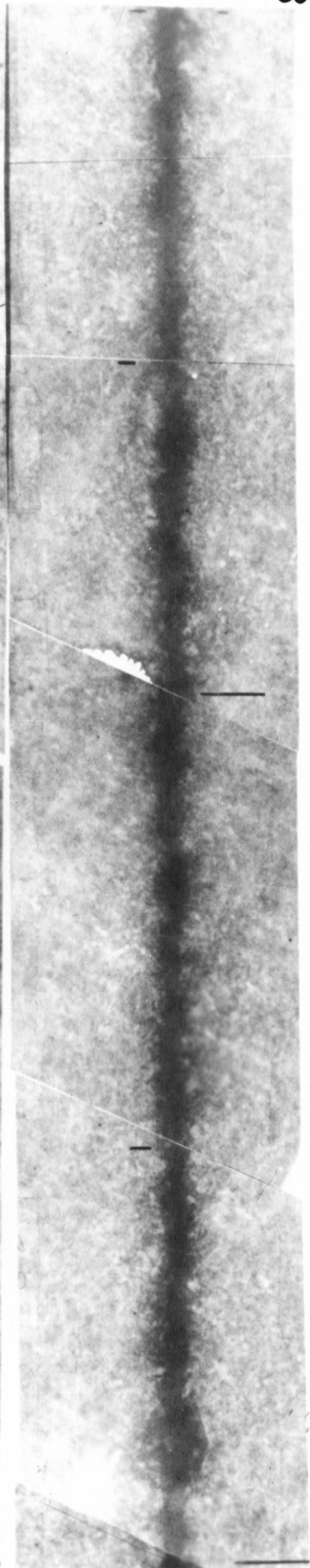
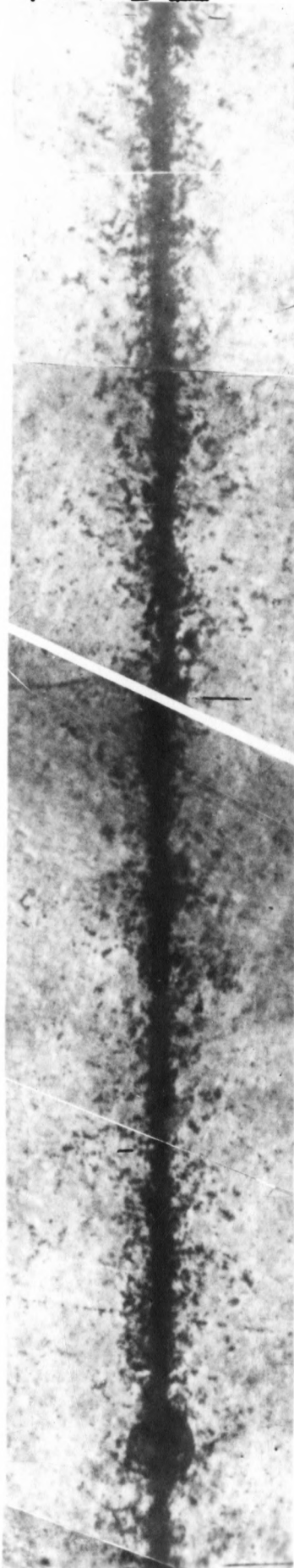
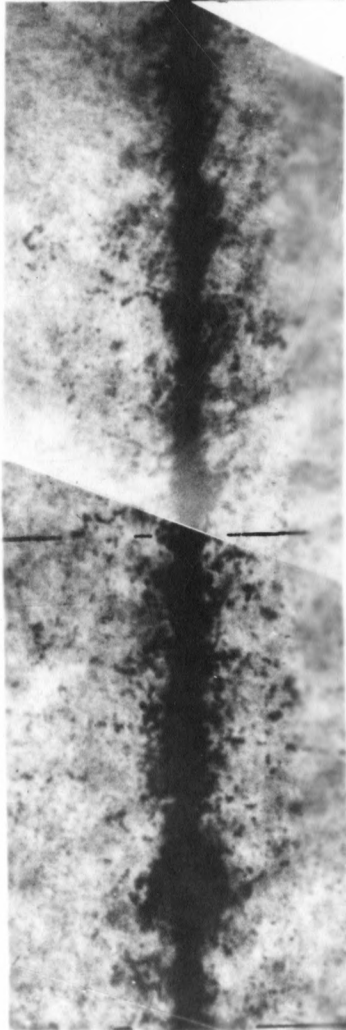
818



918

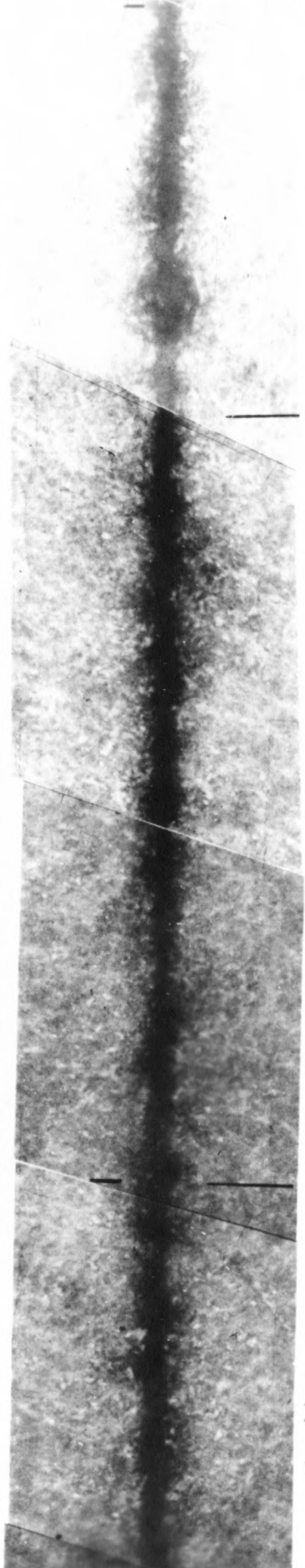
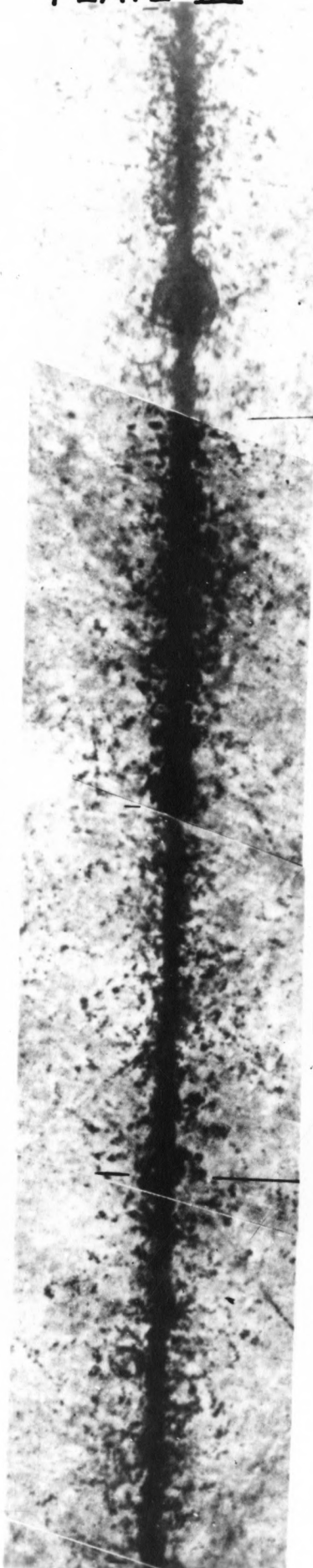
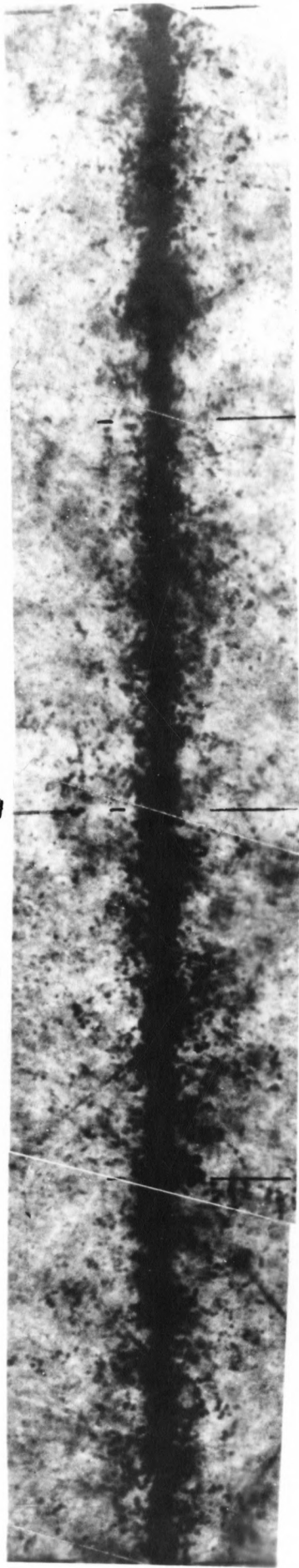


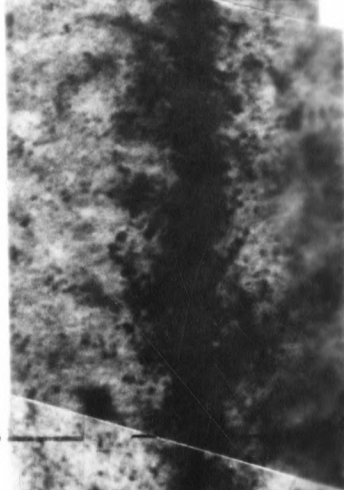
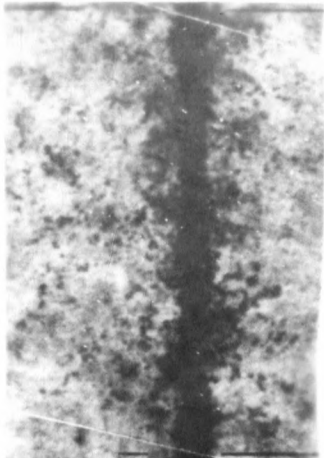
1123



1354

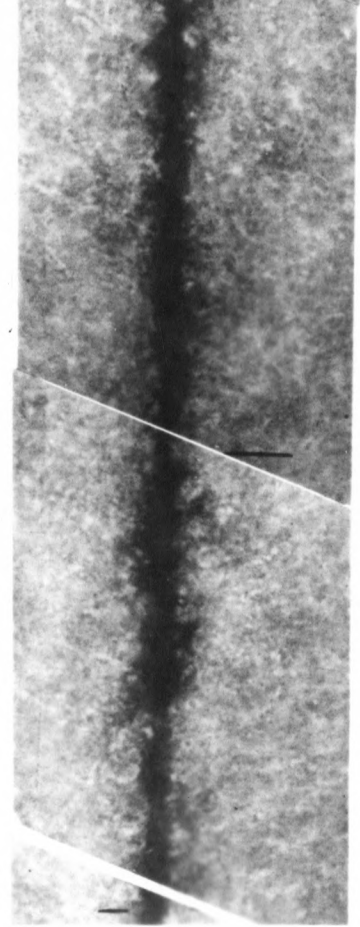
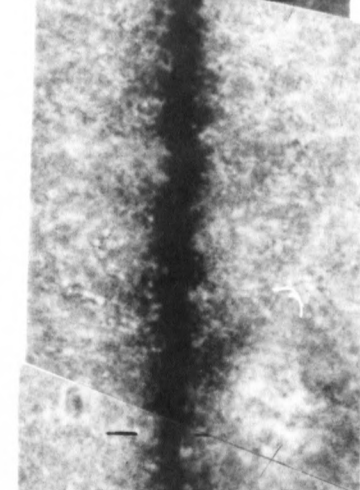
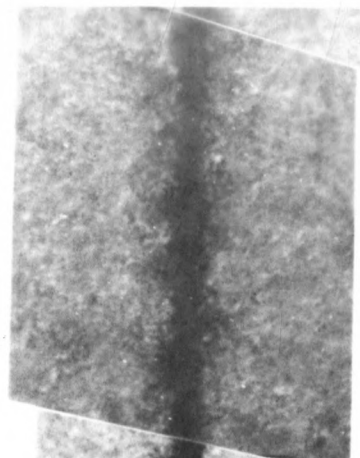
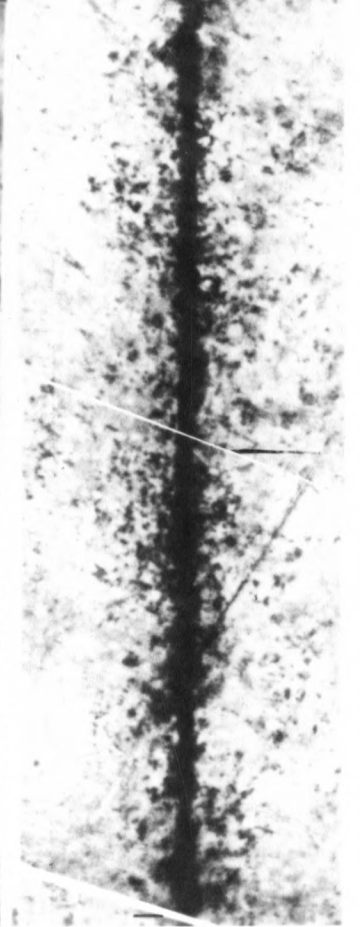
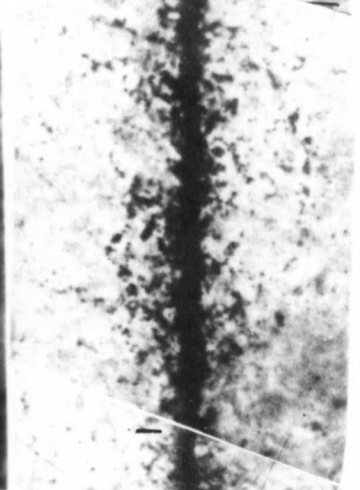
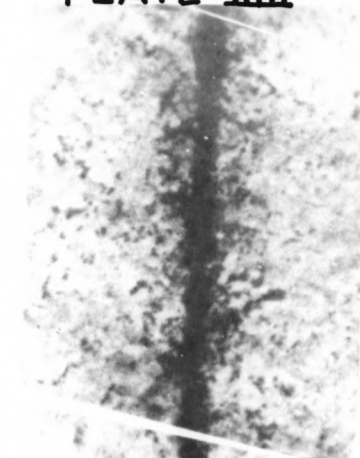
1550





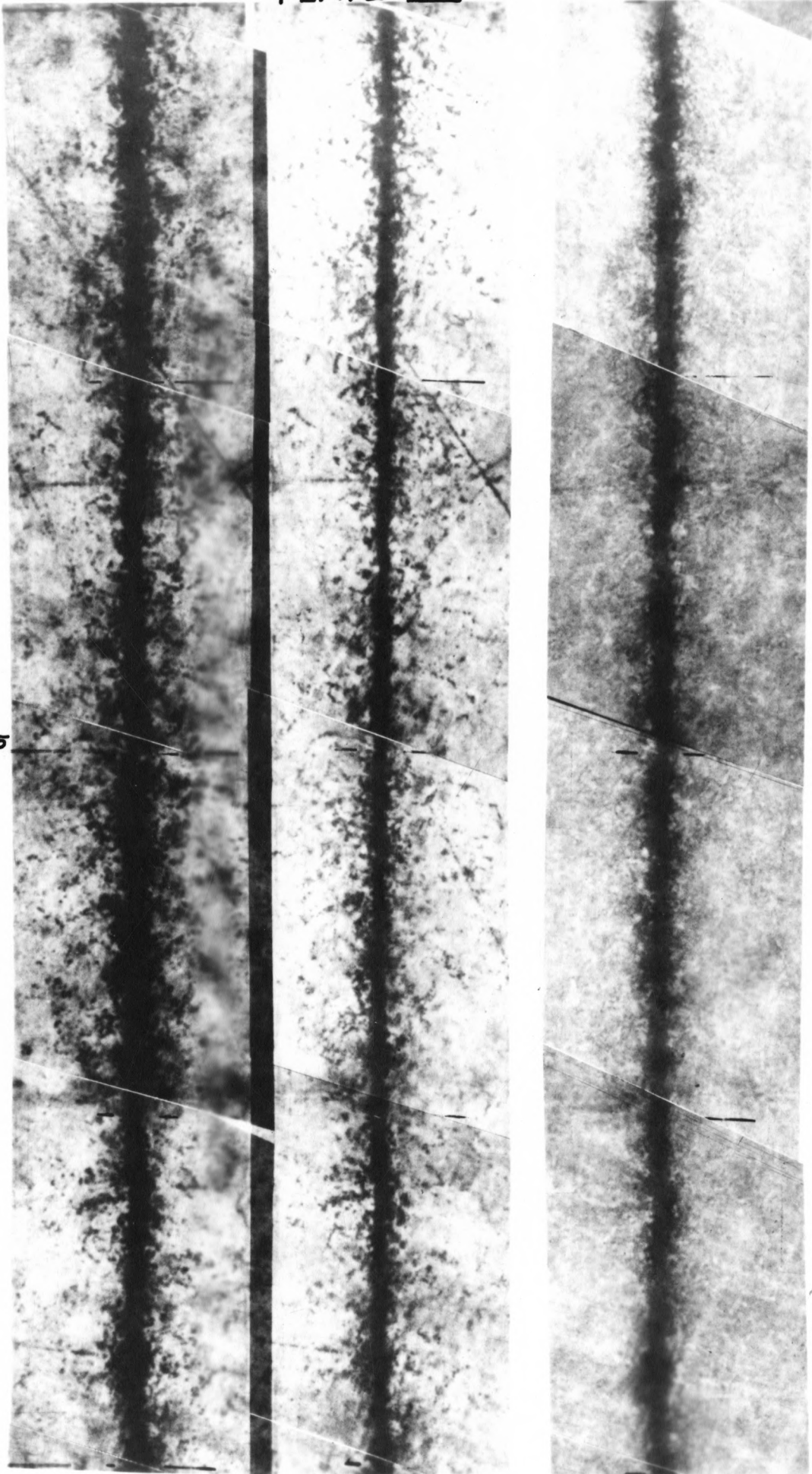
1776

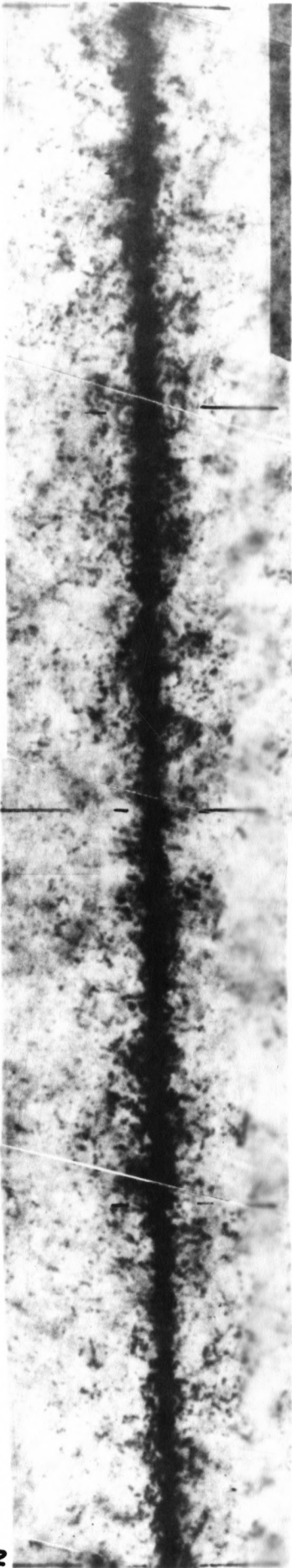
2009



2245

2416

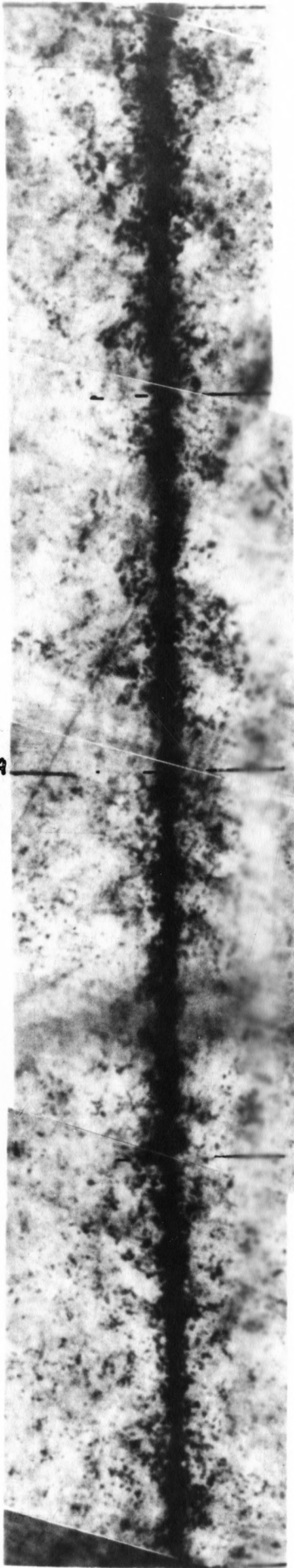




2644

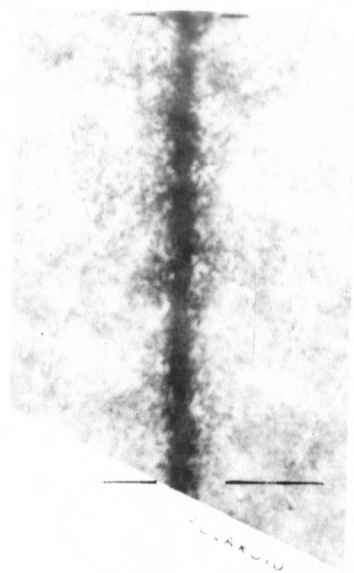
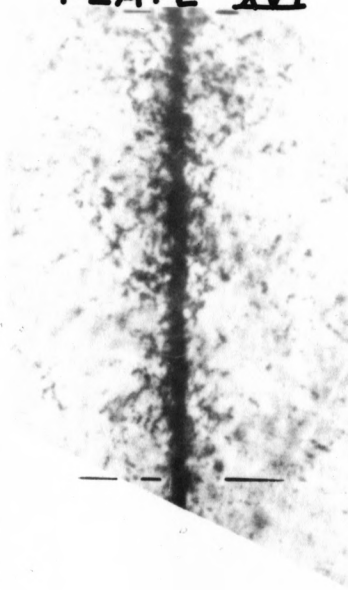
2862



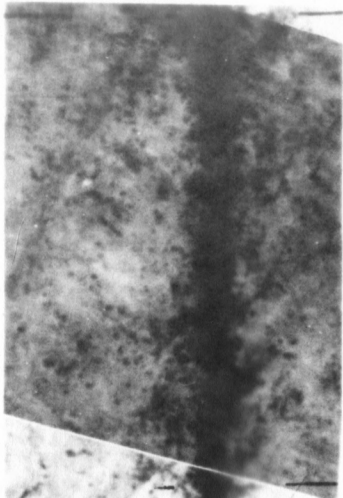


3084

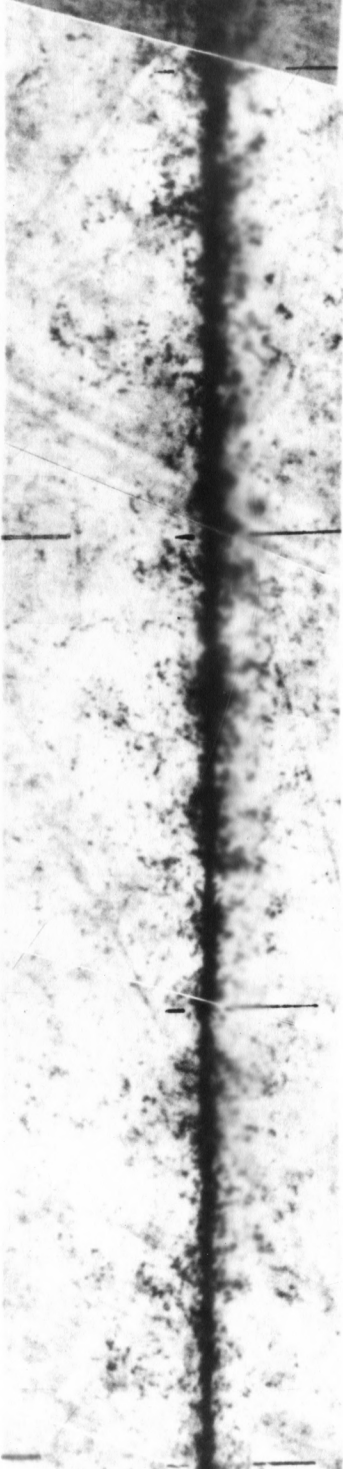
3316



3316



3542



3748

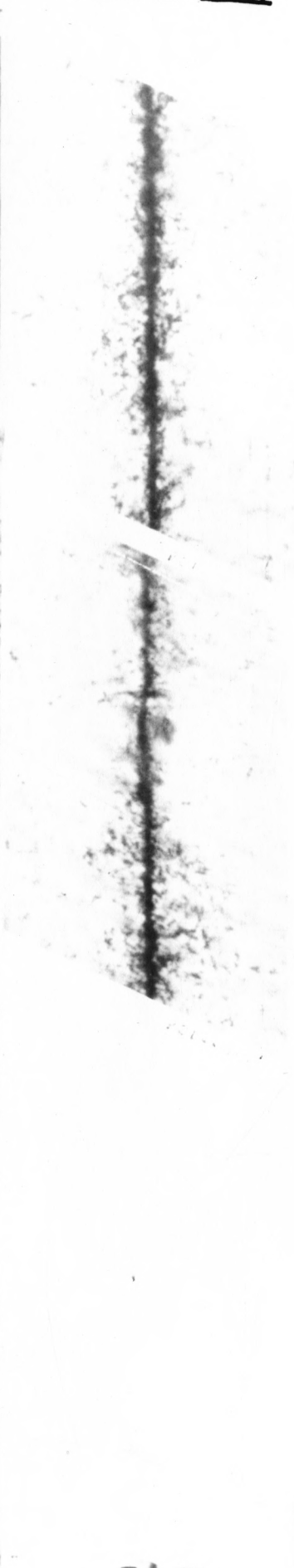
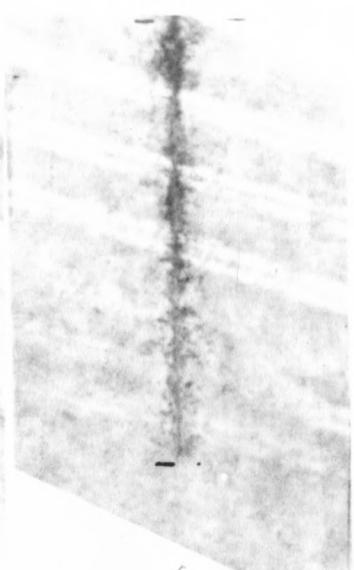
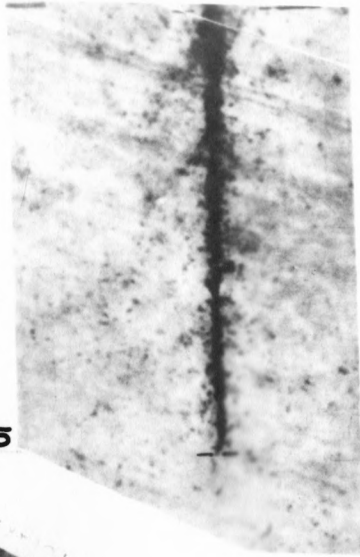
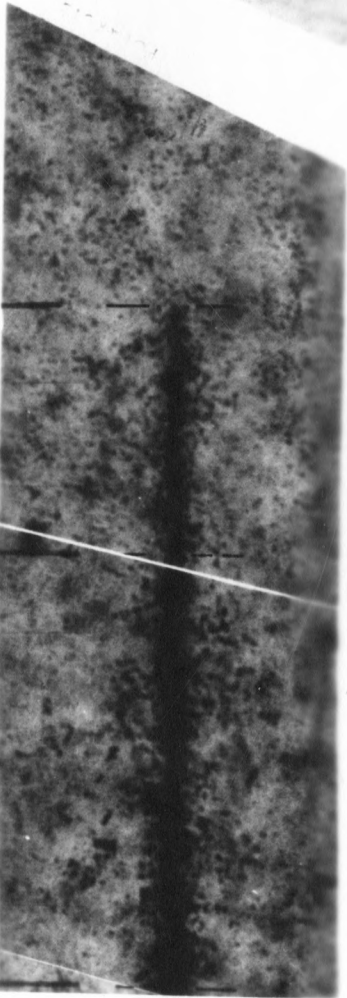


PLATE XVIII

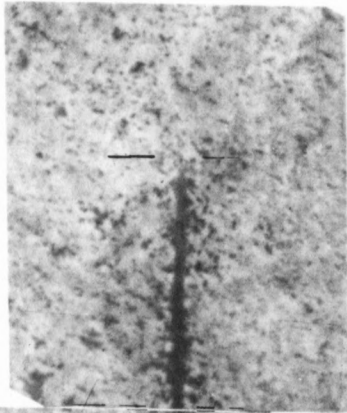
3855



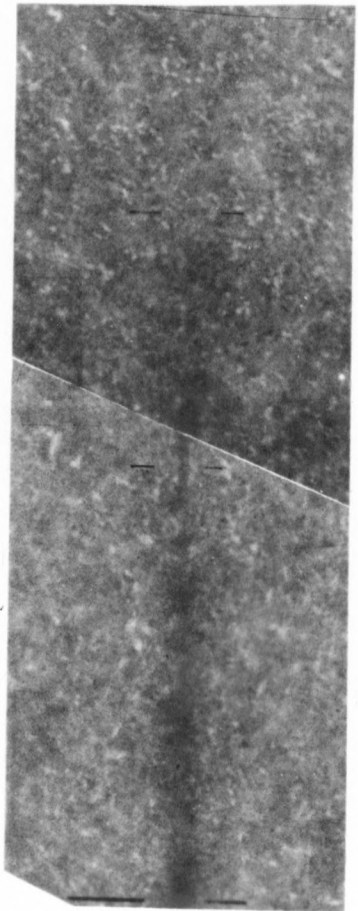
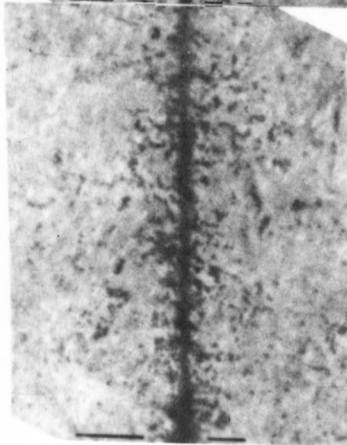
3855

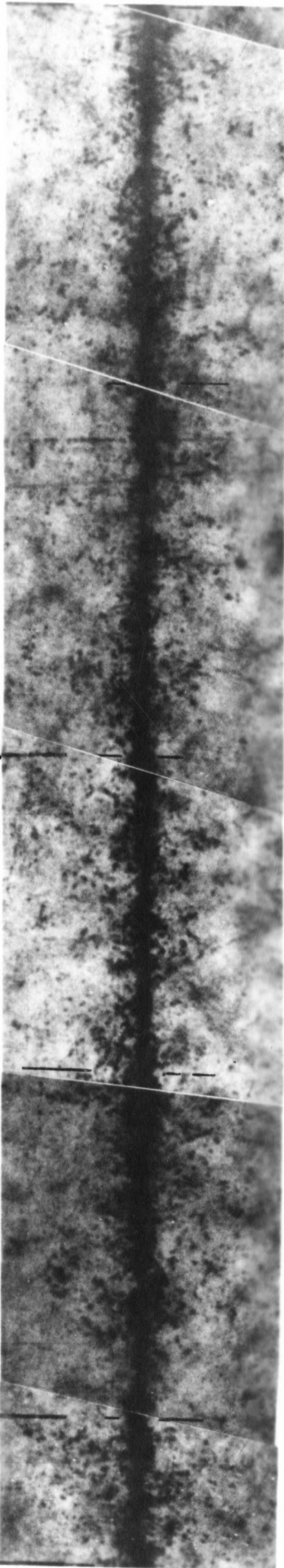


3915



4020





4242

4437

4481

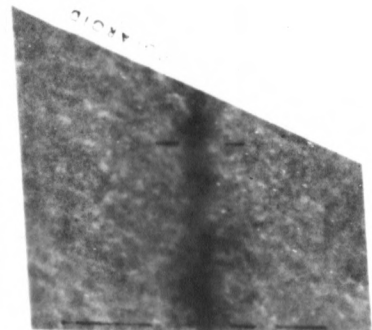
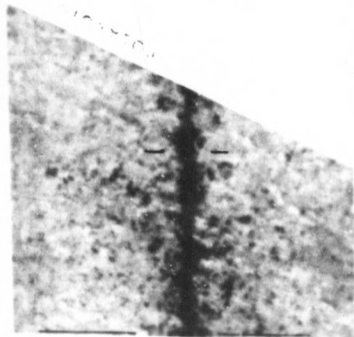
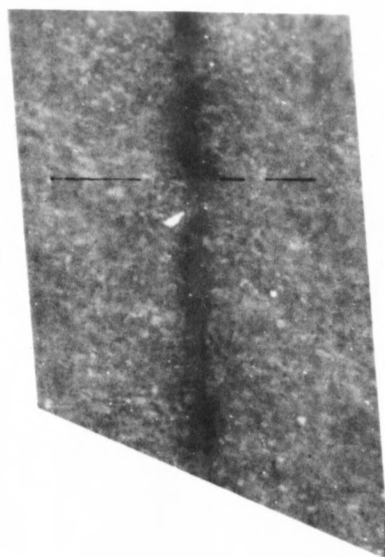
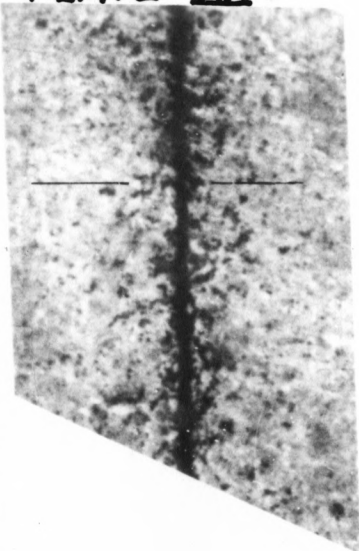
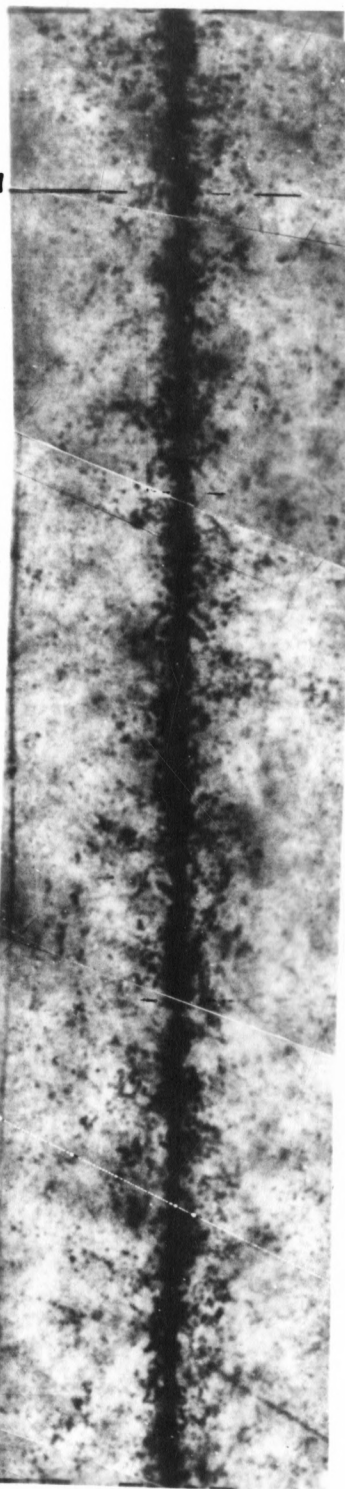


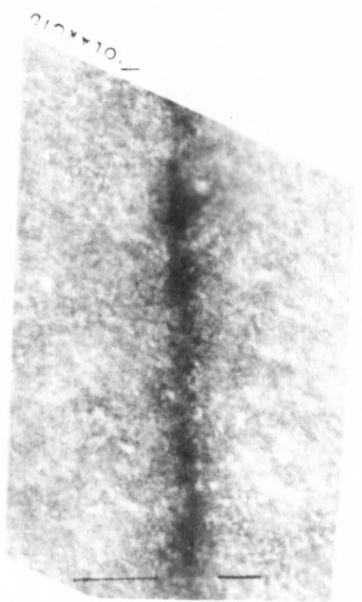
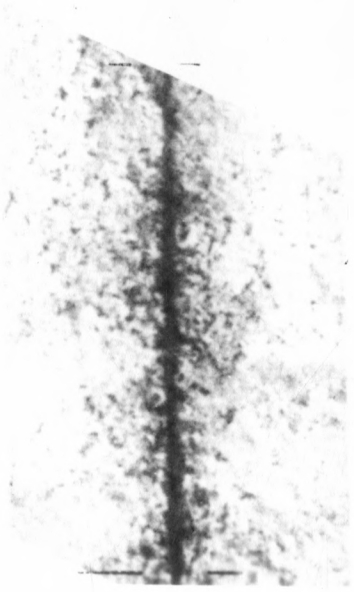
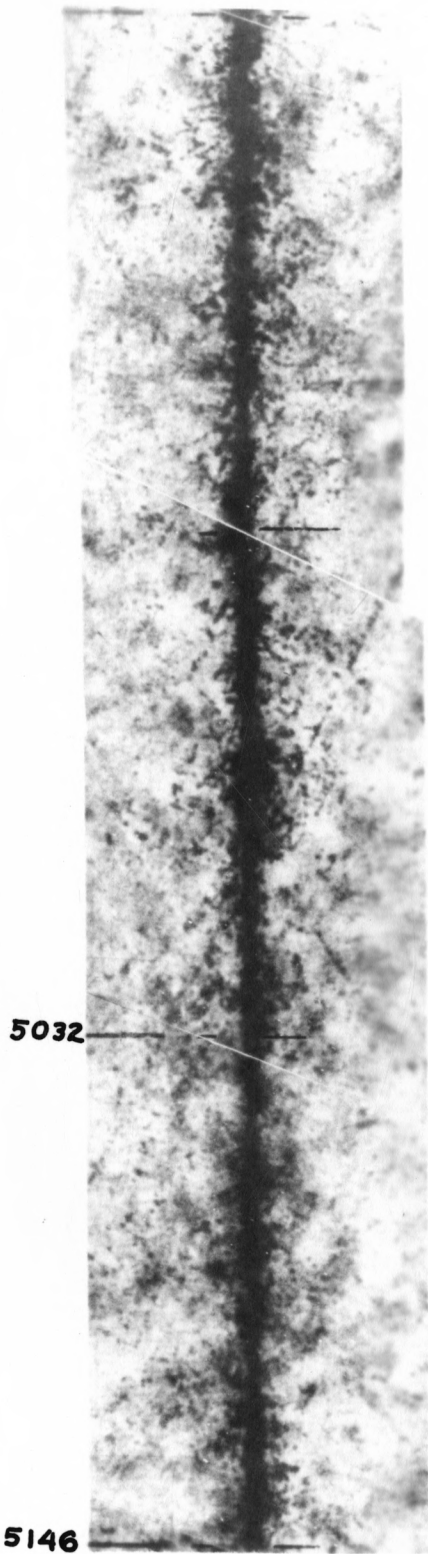
PLATE XX

4481



4794

PLATE XXI



5371

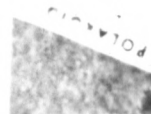
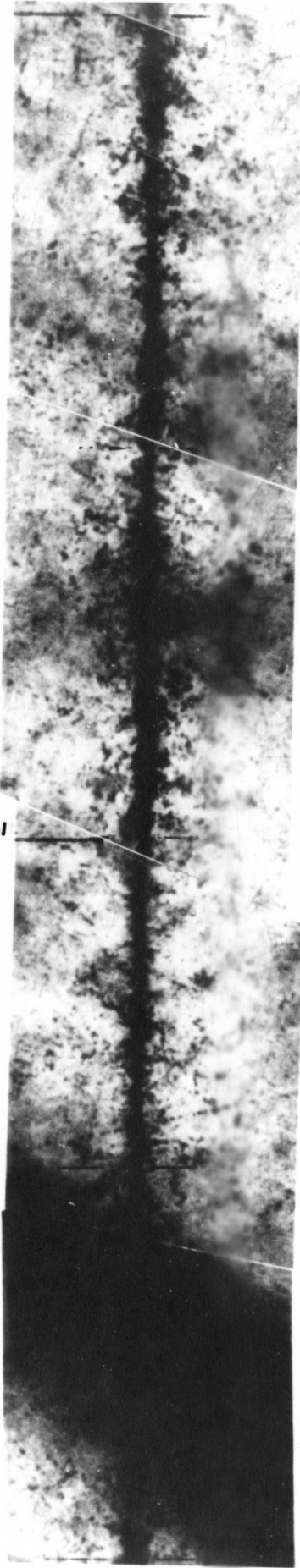
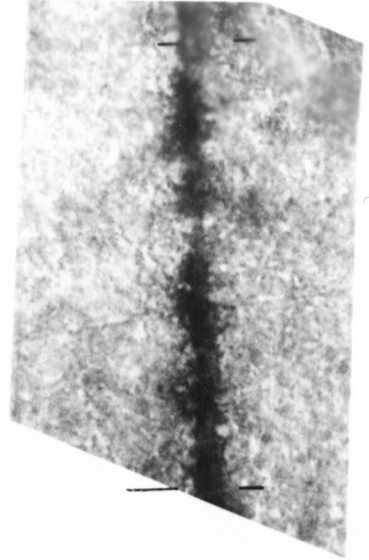
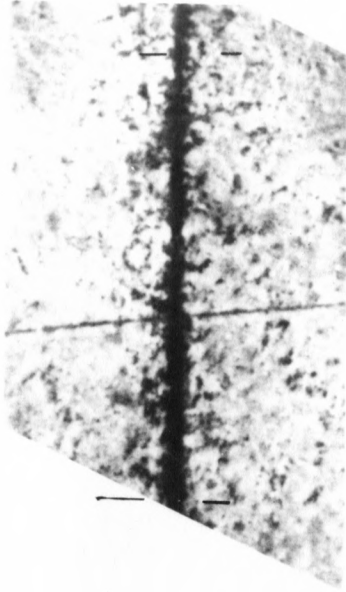
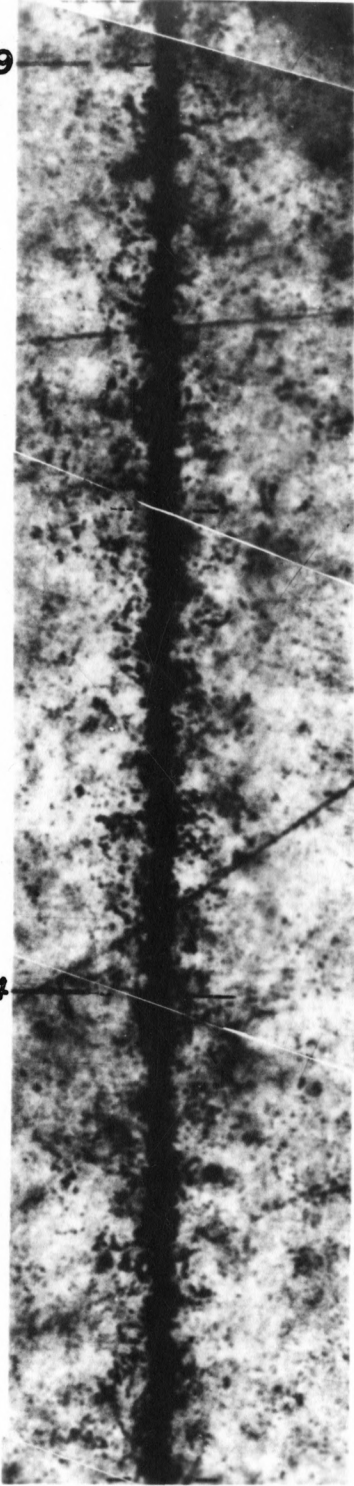
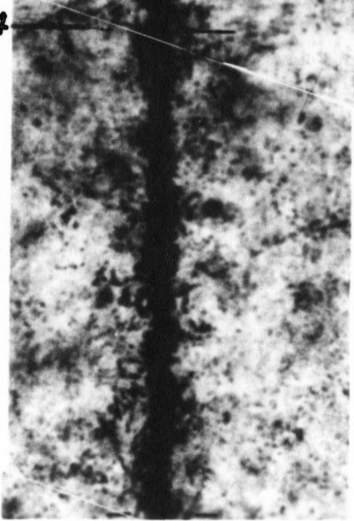


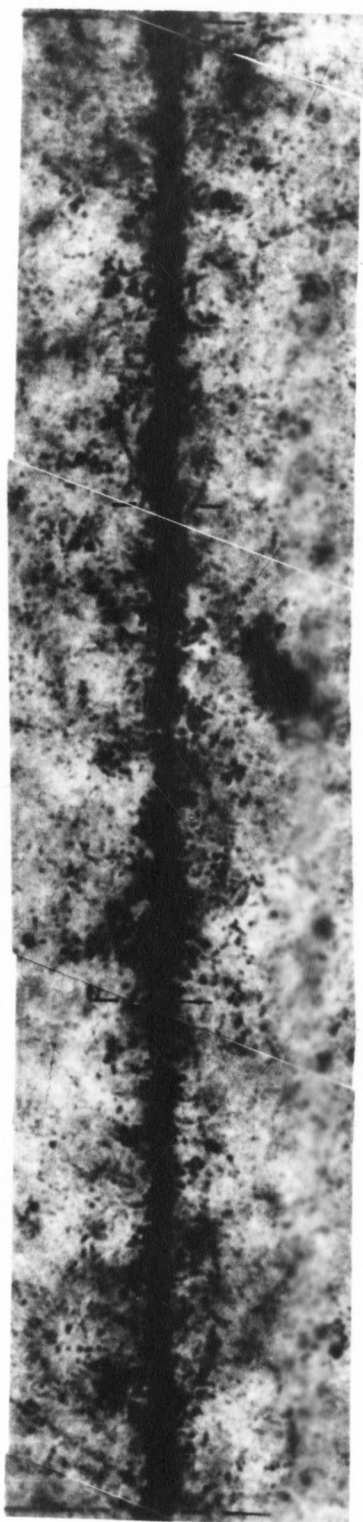
PLATE XXIII

5579



5804





6155

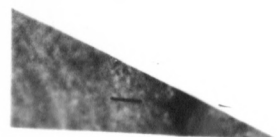
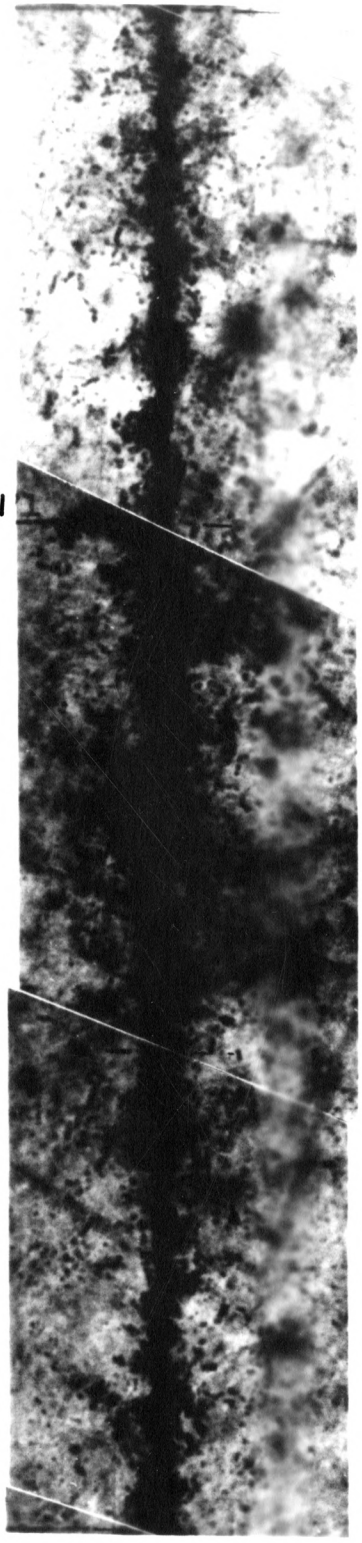
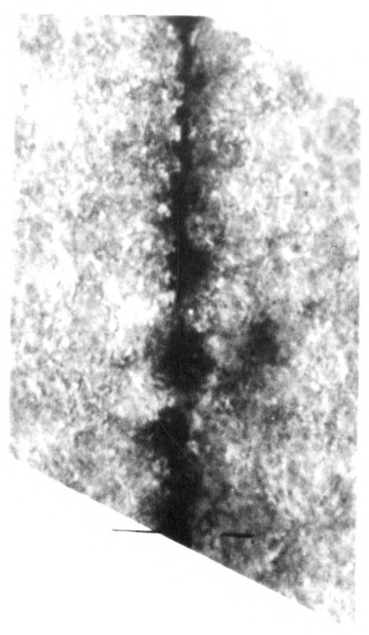
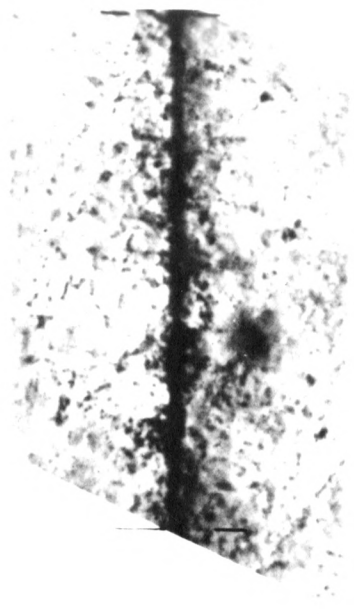


PLATE XXV

6271



6517



6756

6980

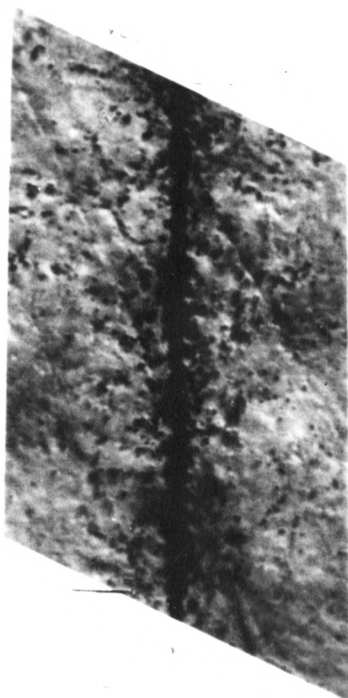
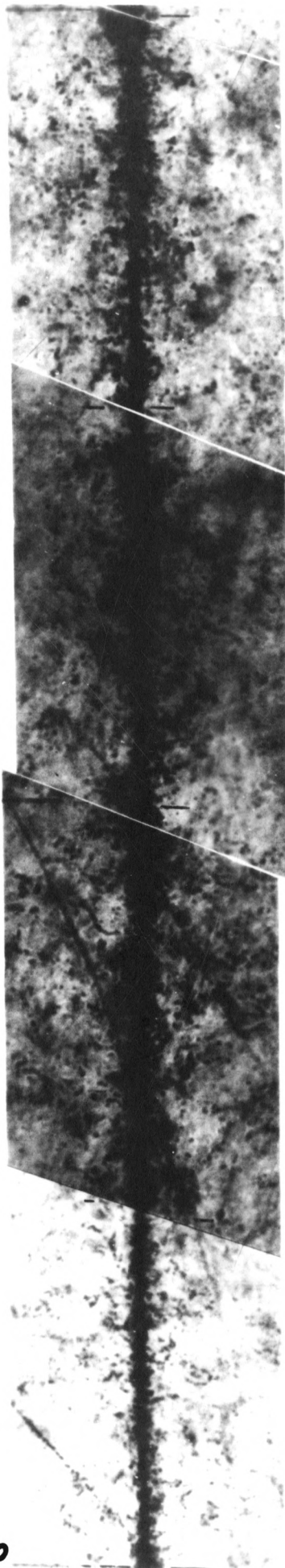
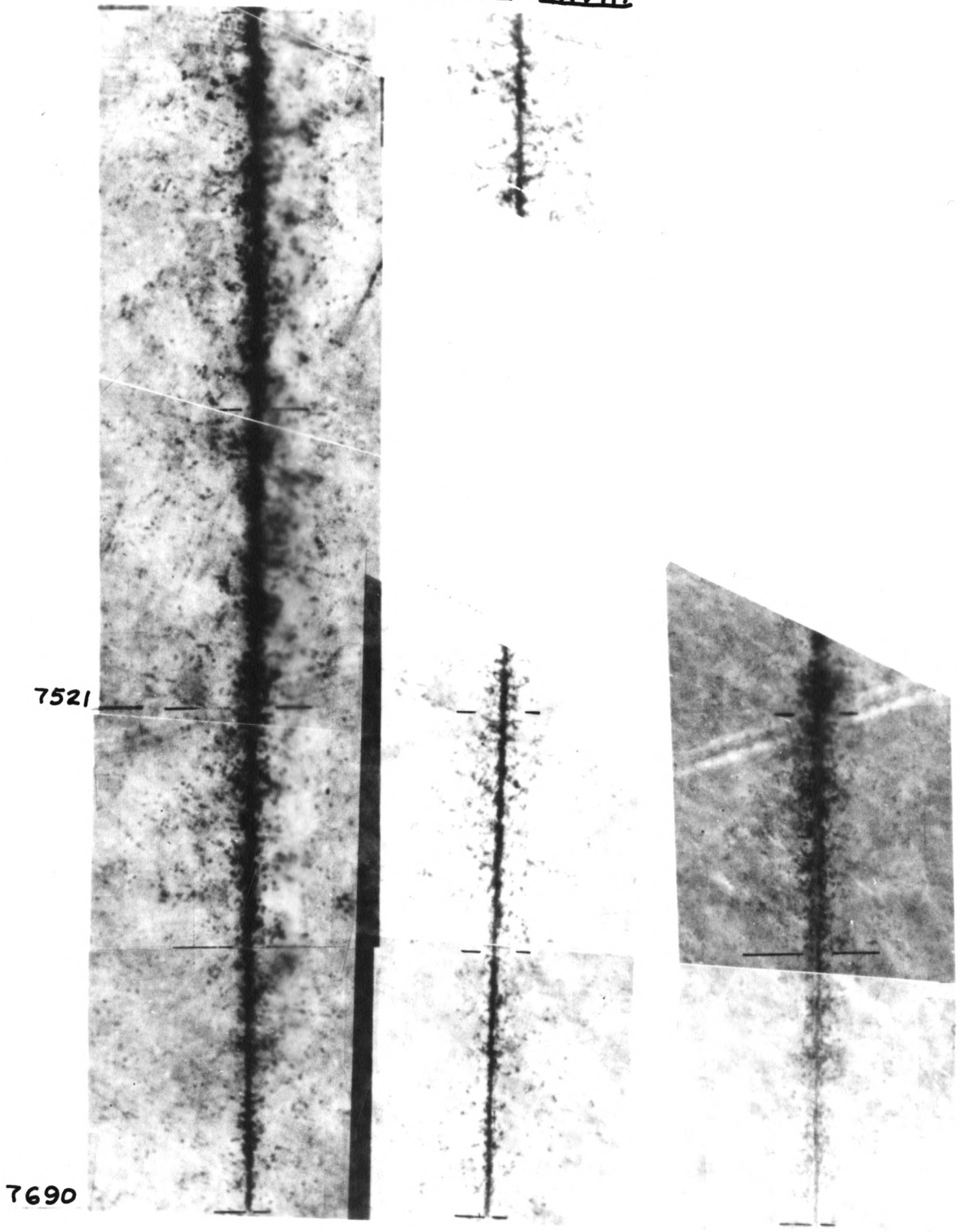


PLATE ~~XXVII~~



PLATE XXVIII



ACKNOWLEDGMENTS

Deep appreciation is expressed to Dr. Robert Katz for his guidance and most helpful advice.

Also, appreciation is expressed to Mr. Earl Hoffman for his participation in track width measurements and to my wife for her production of the plates.

Mr. E. Obi's original observation of the phenomenon of track disappear under phase contrast observation which led to the research embodied in this paper is acknowledged.

Appreciation is also expressed to the Research Corporation for supplying necessary funds to carry out this research and to Dr. David Haskin and Prof. R. D. Hill who furnished the processed plates.

LITERATURE CITED

LITERATURE CITED

- (1) Bizzeti, P., and M. Della Corte.
On the thinning down of tracks of heavy nuclei in nuclear emulsions.
Il Nuovo Cimento. 11:317. 1959.
- (2) Bradt, H. L., and B. Peters.
Investigation of the primary cosmic radiation with nuclear photographic emulsions. Phys. Rev. 74:1828-1837. 1948.
- (3) Cline, D. B.
Theory of heavy nuclear tracks in electron sensitive nuclear emulsions with an application to the track of a Dirac monopole. Kansas State University. 1960
- (4) Cuer, P., and J. Lonchamp.
Sur l'epaisseur des traces des noyaux lourdes dans les emulsions nucleaires. C. R. Acad. Sci. (Paris), 236:70-72. January 5, 1953.
- (5) Demers, P.
Ionographie. Les Presses Universitaires de Montreal, 1958. 252-254.
- (6) Evans, D., and R. R. Hillier.
Remarks upon the densitometry of the tracks of heavy nuclei in nuclear emulsion. Il Nuovo Cimento 20: 1961.
- (7) Frier, P., E. J. Lofgren, E. P. Ney, and F. Oppenheimer.
The heavy component of primary cosmic rays. Phys. Rev. 7:1818-1827. 1948.
- (8) Hoang, T. F., and D. Morellet.
Sur l'ameincissement des trajecteries des noyaux lourds dans l'emulsion photographique. C. R. Acad. Sci. (Paris) 231:695-697. 1950.
- (9) Gegauff, G.
Contribution a l'etude photographique et methodologique des diminsions transversale de traces d'ions dans les emulsions ionographiques. Annales de Physique. 5:1027-1084. 1960.
- (10) Katz, R., and D. Parnell.
Two proposed experiments for the detection of the Dirac monopole. Phys. Rev. 116:236. 1959
- (11) Lonchamp, J. P.
Sur le developpement induit le long des traces nucleaires dans l'emulsion photographique. J. Phys. Radium. 14:433-438. 1953.
- (12) Lonchamp, J. P.
Sur les courbes parcours - energie des ions positifs de charge superieure a l'dans les emulsions nucleaires. J. Phys. Radium. 14:89-95. 1953.

- (13) Mott, N. F.
The scattering of fast electrons by atomic nuclei. Roy. Soc. London,
Proc. 124:425-442. 1929.
- (14) Parnell, D. R.
The search for a unit magnetic pole in nuclear emulsions. Kansas State
University. 1959.
- (15) Perkins, D. H.
Emission of heavy fragments in nuclear explosions. Roy. Soc. London,
Proc. 203:405. 1950.
- (16) Powell, C. F., P. H. Fowler, and D. H. Perkins.
The study of elementary particles by the photographic method. Pergamon
Press, 1959. 83-86, 172-178.
- (17) Skjeggsted, O.
The nature of the taper tracks of heavy ions in nuclear emulsion.
Il Nuovo Cimento, June 16, 1958, 927-935.
- (18) Waldskog, B., and O. Mathiesen.
Ark. F. Fys. 17, No. 25. 1960.

APPENDICES

TABLE OF CONTENTS OF APPENDICES

Appendix I:	Abbe Theory of Image Formation in a Microscope	63
Appendix II:	Fraunhofer Diffraction Pattern in a Microscope	69
Appendix III:	Phase Object Microscopy.	79
Appendix IV:	Phase Contrast Microscopy.	84
Appendix V:	Mathematical Treatment of the Phase Microscope.	94

APPENDIX I

Abbe Theory of Image Formation in a Microscope

Although the formation of an image in a microscope rendered in terms of geometrical optics appears simple; the physical process and explanation in terms of physical optics is extremely complex. Most objects are usually non-luminous and, thus, require an auxiliary system for their illumination. Due to diffraction taking place at the aperture of the illuminating system (condenser), each element of the source gives rise to a diffraction pattern in the object plane of the microscope. Those diffraction patterns that have centers on points that are sufficiently close to each other will partially overlap; consequently, the light variations at neighboring points of the object plane are in general partially correlated. Some of this light will be transmitted with or without a change in phase through the object; the remainder will be scattered, reflected, or absorbed. Consequently, it is generally impossible to obtain a faithfully enlarged picture depicting all the small scale structural variations of the object by means of a single observation or by the use of one particular optical arrangement. Thus, various methods of observation have been developed, each being suitable for the study of certain type objects, or designed to accentuate particular features.

Image formation in the microscope may be regarded from three different viewpoints with respect to illumination; the two extreme cases of completely incoherent (1) and perfectly coherent (2) light and the general case of partially coherent light (3). Neither partially coherent nor incoherent illumination bear great relevancy with respect to the subject of this discussion. We therefore consider the case where light emerging from the object may be treated as strictly coherent.

This situation is approximately realized when a thin object of relatively simple structure is illuminated by light issuing from a sufficiently small source via a condenser of low aperture (Kohler's Illumination).

The first satisfactory theory of resolution with coherent illumination was promulgated by E. Abbe (4). According to Abbe, the object acts as a diffraction grating, so that not only every element of the aperture of the objective, but also every element of the object must be taken into account in determining the complex (amplitude-phase) disturbance at any particular point in the image plane. Expressed mathematically (5), the transition from the object to the image involves two integrations, one extending over the object plane, the other extending over the aperture. In Abbe's theory, diffraction by the object is first considered and the effect of the aperture is taken into account in the second integration. An alternate procedure (6) in which the order is reversed leads to the same result.

To illustrate Abbe's theory, consider the imagery of a regular grating consisting of opaque and transparent elements illuminated by restricted Kohler illumination (7), (8), (9), where, in effect a point source is located in the back focal plane of the condenser (Plate I-1). This gives rise to a single collimated beam of light incident normally to the object plane. The light strikes the grating G and is diffracted by it. If the objective possesses a sufficiently large aperture, the diffracted beams are collected in the back focal plane of the objective. The back focal plane of the objective is conjugate to the source; hence, the diffraction maxima are in focus in this surface and constitute a Fraunhofer diffraction pattern of the grating. In figure-1, the maxima (spectra of successive orders) of this pattern are denoted by $\dots S_{-2}, S_{-1}, S_0, S_1, S_2 \dots$. Every point in the back focal plane can now be regarded (utilizing Huygen's Principle) as a center of a coherent secondary

disturbance, whose strength is proportional to the amplitude at that point. The light waves that precede from these secondary sources will then interfere with each other giving rise to the image of the object in the plane conjugate to the grating (the image plane of the objective).

Since the disturbance in the region of the zero order maximum for the grating closely resembles the pattern for a single aperture whose width is equal to the overall width of the grating, the disturbances which pass from these patterns to the image plane should yield similar intensity distributions in the image plane. Noting that the single aperture would give uniform illumination across the image plane, the light associated with the zero order maximum must produce uniform illumination across the image plane. Combining the disturbances from the zero order and from one of the first order maxima for the grating yields, across the image plane, the cosine amplitude distribution, depicted in figure-1(a), plus a uniform amplitude. In figure-1, first and higher order maxima are admitted on both sides of the axis. The effect of these maxima of higher orders is to cause the intensity distribution across the image plane to approach the square wave form, depicted in figure-1(b), which is exactly the form of the intensity distribution immediately behind the grating. That is, the image approaches perfect reproduction of the object as the number of diffracted orders collected by the objective increases. Although this perfect imagery can be obtained if and only if all the diffracted orders are collected by the objective (an impossibility due to the finite aperture of the objective), the periodicity of the grating is reproduced in the image if the objective collects only the light in the zero order and one first order maximum. Since resolution of the grating rulings does not exist with the zero order alone, the collection of the zero order and one first order is the minimum requirement

for resolution of the grating (Abbe's Principle). Exclusion of some of the spectra may result in completely false detail appearing in the image; however, for practical purposes it is sufficient that the aperture shall be large enough to admit all those spectra that carry an appreciable amount of the energy. A finer grating will have a larger angle of diffraction for a given order; thus, the collection of the necessary maxima requires an objective that will admit a wider cone of light. Hence, to resolve finer gratings one must employ an objective of larger numerical aperture. If the zero order maximum is removed from the light passing through the objective, then one would observe a grating consisting of white rulings against a dark background (10). This isolation of the zero order is utilized in central dark-field illumination (11).

REFERENCES

- (1) M. Born, and E. Wolf, "Principles of Optics", (1959, Pergamon Press, New York), pp. 417-418, pp 519-521.
- (2) M. Born and E. Wolf, *ibid.*, pp. 418-423, pp.521-523.
- (3) M. Born and E. Wolf, *op. cit.*, pp. 523-529
- (4) E. Abbe, *Archiv F. Mikroskopische Anat.*, 9 (1873) p.413.
- (5) M. Born and E. Wolf, *op. cit.*, pp. 418-423.
- (6) Lord Rayleigh, *Phil. Mag.* (5), 42 (1896), p. 167.
- (7) M. Born and E. Wolf, *op. cit.*, pp. 521-523.
- (8) R. S. Longhurst, "Geometrical and Physical Optics", (1957, Longmans, Green and Co., New York), pp. 289-290.
- (9) J. Belling, "The Use of the Microscope", (1930, McGraw-Hill Book Co., Inc., New York), pp. 66-74.
- (10) J. Strong, "Concepts of Classical Optics", (1958, W. H. Freeman and Co., San Francisco), pp. 527-528.
- (11) R. S. Longhurst, *op. cit.*, pp. 294-295.

EXPLANATION OF PLATE I-1

Schematic illustration of a microscope system, illustrating Abbe's theory of image formation.

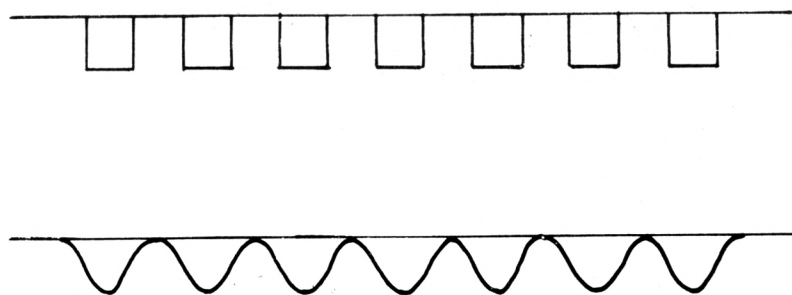
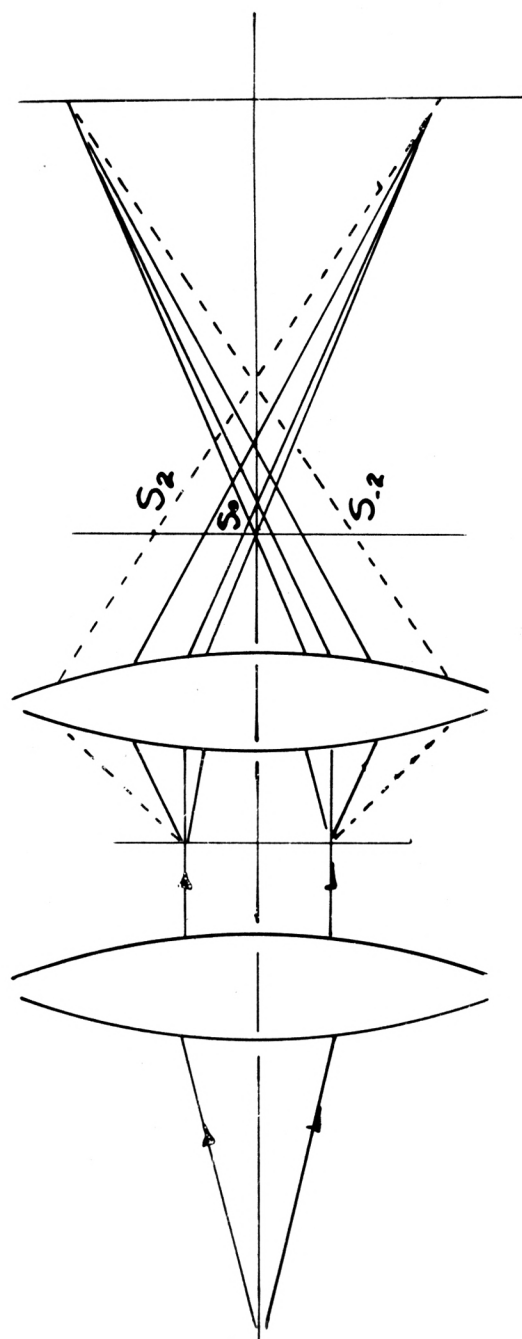


PLATE I-1



APPENDIX II

Fraunhofer Diffraction Pattern in a Microscope

To inquire into the relationship between object and its Fraunhofer diffraction pattern in the back focal surface of the objective of a microscope, consider the arrangement depicted in Figure-1 of Plate II-1. If the lenses L_1 and L_2 possess extremely large apertures and the diffracting screen at Σ is removed, the plane W is approximately focused on the axis at S. If a diffracting screen containing a slit aperture is interposed at Σ , limiting the extent of the plane wave, a Fraunhofer pattern is formed on the receiving screen S. The complex amplitude $\phi(\theta)$ at a point on the back focal surface of lens L_2 (objective), corresponding to the angle θ , is obtainable from Kirchoff's Diffraction Formula (1), (2), (3), (4), and is expressed by the relation

$$\phi(\theta) = \int_{-l}^{+l} a e^{ikx \sin \theta} dx \quad (1)$$

where a is a constant and $K = \frac{2\pi}{\lambda}$ is the wave propagation number (space frequency). If the disturbance passing through the slit aperture is not a uniform plane wave but is a function of x , then a is replaced by $f(x)$ in relation (1), yielding

$$\phi(\theta) = \int_{-l}^{+l} f(x) e^{ikx \sin \theta} dx \quad (2)$$

In order to expand the definition of the function $f(x)$ in relation (1) from a function possessing only limited periodicity to one that possess an infinite periodicity, we have to go through the following sequence of operations.

Consider the function $f(x)$, if it obeys sufficient continuity conditions, it may be represented over a range $-l \leq x \leq l$ by the Fourier expansion (5)

$$f(x) = \sum_{n=-\infty}^{n=+\infty} C_n \exp\left(\frac{in\pi x}{l}\right) \quad (3)$$

where

$$C_n = \frac{1}{2l} \int_{-l}^{+l} f(x) \exp\left(-\frac{in\pi x}{l}\right) dx \quad (4)$$

Hence,

$$f(x) = \sum_{n=-\infty}^{n=+\infty} \frac{1}{2l} \int_{-l}^{+l} f(x') \exp\left[\frac{in\pi}{l}(x-x')\right] dx' \quad (5)$$

where the summation on the right hand side represents $f(x)$ in the range $-l \leq x \leq l$.

Now the n th harmonic in this series has wave length $\lambda_n = \frac{2l}{n}$ and in terms of the wave propagation number $k = \frac{2\pi}{\lambda}$, one has $k_n = \frac{n\pi}{l}$. Similarly $k_{n+1} = \frac{(n+1)\pi}{l}$.

Hence $k_{n+1} - k_n = \frac{\pi}{l} \equiv \Delta k$. Thus

$$f(x) = \frac{1}{2\pi} \sum_{n=-\infty}^{n=+\infty} \Delta k \int_{-l}^{+l} f(x') e^{i\{n\pi k(x-x')\}} dx' \quad (6)$$

Now $n\pi k = k_n$ and as $l \rightarrow \infty$, $\Delta k \rightarrow 0$, and

$$f(x) = \frac{1}{2\pi} \int_{-\infty}^{\infty} dk \int_{-\infty}^{\infty} f(x') e^{ik(x-x')} dx' \quad (7)$$

$$f(x) = \frac{1}{\sqrt{2\pi}} \int_{-l}^l g(k) e^{ikx} dk \quad (8)$$

where

$$g(k) = \frac{1}{\sqrt{2\pi}} \int_{-\infty}^{\infty} f(x) e^{-ikx} dx \quad (9)$$

Equation (8) indicates that the function $f(x)$ is represented by an integral of simple harmonic terms whose amplitudes are given by equation (9). When two functions such as $f(x)$ and $g(k)$ are related in this way, each is said to be the Fourier Transform of the other. Since $f(x)$ is zero outside of the aperture of the slit, the limits of integration of relation (2) may be extended to $\pm\infty$ and, on writing $k \sin \theta = k_x$, and noting $\phi = \phi(k_x)$, and introducing the constant $\frac{1}{\sqrt{2\pi}}$, relation (2) becomes

$$\phi(k_x) = \frac{1}{\sqrt{2\pi}} \int_{-\infty}^{\infty} f(x) e^{ik_x x} dx \quad (10)$$

In the light of relations (8) and (9), relation (10) implies that

$$f(x) = \frac{1}{\sqrt{2\pi}} \int_{-\infty}^{\infty} \phi(k_x) e^{-ik_x x} dk_x \quad (11)$$

Thus, the Fraunhofer pattern in the back focal plane of the lens L_2 is the Fourier transform of the amplitude across the diffracting aperture and vice versa. Equation (10) says that the plane wave passing through the aperture may be represented from the viewpoint of the receiving screen in the back focal plane of the objective as a continuous distribution of waves each bearing a

given K_x whose amplitudes are given by relation (11). Thus equations (10) and (11) states that of a wave front is limited in "width" it can be analyzed into a continuous distribution of waves in all "directions" (see Figure-2 of Plate II-1), the angular spread becoming smaller as the width of the wave front is increased. Therefore, in Figure-1, where the incident plane wave W is limited by the slit Σ , it becomes equivalent to a continuous distribution of plane waves traveling in all directions through the objective (lens L_2), the relative amplitudes being given by the relative amplitudes on the receiving screen S , where the Fraunhofer pattern on screen S is the Fourier transform of the amplitude of the incident plane wave across the diffracting aperture of the slit.

The formation of a continuous distribution of plane waves traveling in all directions by limiting a plane wave in width, as depicted in Figure-2, implies that a microscope may never completely duplicate the object in the image plane of the microscope, since the higher wave numbers (k_x 's) will completely miss the aperture of the objective. Figure-3 of Plate II-1 compares the intensity distribution viewed utilizing a finite aperture with the intensity distribution that would be observed with an infinite aperture in the optical plane (conjugate to the image plane of the microscope shown in Figure-1).

For a wave limited in two dimensions a similar analysis yields the relations,

$$\phi(k_x, k_y) = \frac{1}{2\pi} \int_{-\infty}^{\infty} f(x, y) e^{i(k_x x + k_y y)} dx dy \quad (12)$$

$$f(x, y) = \frac{1}{2\pi} \int_{-\infty}^{\infty} \phi(k_x, k_y) e^{-i(k_x x + k_y y)} dx dy \quad (13)$$

In Abbe's theory images are formed in the image plane by the interference of light from the diffracting maxima located in the back focal surface of the

objective. Let us contemplate a more complicated object in place of the simple slit object in Figure-1. Consider as the fundamental object structure, in our microscope, one which, if illuminated by a plane wave traveling along the optical axis of the system (Kohler's illumination), will yield just two maxima in the back focal plane of the objective, plus a central minimum of maximum (6), the maxima being symmetrically located on each side of the optical axis of the system. Two coherent sources behind the objective will yield by combination a sinusoidal variation of amplitude across the image plane. In Abbe's theory, object and image structure are identical if all of the diffraction maxima formed by the object contribute to the image. Thus, it follows, that the fundamental object structure must be a sinusoidal structure; that is, the transmitted amplitude varies sinusoidally across the object plane. In general, the diffraction pattern which an object produces behind the objective is a superposition of pairs of maxima of the type mentioned above (7). So it follows, that any object can be regarded as the superposition of a series of sinusoidal structures; that is, the object is analyzed into spatial frequencies in much the same manner that a complex periodic motion is analyzed into components of various temporal frequencies. If the microscope is to resolve a given spatial frequency in the object, the corresponding diffraction maxima must be transmitted by the objective. The higher frequencies in the object yield diffraction maxima in the outer zones of the objective aperture and if some maxima are not admitted because the objective aperture is too small, the corresponding spatial frequencies are not incorporated into the image. Thus, the previously discussed square wave grating can be analysed into spatial frequencies in the same manner as a complex wave form viewed in an oscilloscope can be analysed into sine waves and, in each case, the inclusion of more "frequency" terms gives a closer approach to the square wave form.

Since each component of the object yields maxima in directions inclined at a given angle to the optical axis of the system, the analysis of the effect of coherent light on the complex object structure described above will correspond exactly to the previously considered analysis of coherent light transmitted by a slit aperture into waves traveling in all directions and that the discussion here can be extended to two dimensions in the same manner as the other was.

In the microscope, the image is formed by the combination of the disturbances from the Fraunhofer pattern which is formed in the back focal plane of the objective. Hence, in the object space, the amplitude across the objective aperture is the Fourier transform of the object structure. In that the aperture is finite in extent, not all of this incident light will be transmitted by the objective. Also, the aberrations of the objective will modify the form of the amplitude distribution that occurs across the objective aperture in the image space, and the image is the transform of this modified amplitude distribution. If the objective were completely aberration free and possessed an infinite aperture then it could accept all frequencies and the image would be a perfect reproduction of the object. A component of the object whose spatial frequency is $1/d$ (whose grating interval is d) will possess a maximum in object space whose direction is given by $d \sin \theta = \lambda$. Since $\sin \theta \leq 1$, components whose spatial frequencies are $> \frac{1}{\lambda}$ cannot be reproduced by any real lens.

To form the best possible image of an object a real lens must strive to fulfill two different functions:

- (1) To yield the maximum possible resolving power; that is, it must strive to collect the widest cone of light from the object.
- (2) To reproduce each spatial frequency faithfully; that is, it must yield identical disturbances across its aperture in the object and image spaces.

Owing to aberrational defects in any lens the second function is never fulfilled exactly and the best compromise between the various aberrations must be chosen. In general, however, the compromise that yields the best resolving power (reproduction of highest possible spatial frequency) is different from the compromise which yields the best possible reproduction of all spatial frequencies.

Another way to examine optical systems suggests itself from the Fourier treatment of diffraction patterns. Optical functions may be equated with the language of communication theory (8), (9) and close counterparts to the elements of electrical circuitry will appear. Communications theory predicts that the condenser of a microscope acts very similar in manner as a low band-pass electrical filter, and that the objective of a microscope is comparable to a wide band-pass electrical amplifier, where as the eyepiece in a microscope may be thought of as an electrical integrator. The analogue treatment of lens as electrical filters allows the field of electronics and its developed mathematical techniques to extend the scope of one's ability to attack optical problems; linear circuit theory is much easier to handle than Kirchoff diffraction integrals. The main difference between optical and electrical networks is that in the former the frequency domain is a space frequency where as in the latter the frequency domain is a time frequency.

REFERENCES

- (1) Page, "Introduction to Theoretical Physics", (Addison and Wesley, New York), pp. 582-595.
- (2) R. S. Longhurst, "Geometrical and Physical Optics", (1957, Longmans, Green and Co., New York), pp. 190-194.
- (3) J. Strong, "Concepts of Classical Optics", (1958, W. H. Freeman and Co., San Francisco), pp. 421-424.
- (4) Joo's "Theoretical Physics", (1959, Haftner, New York), pp. 376-383.

- (5) H. Wayland, "Differential Equations Applied in Science and Engineering", (1957, D. Van Nostrand Company, Inc., New York), pp. 234-235.
- (6) J. Strong, *op. cit.*, pp. 424-425.
- (7) R. S. Longhurst, *op. cit.*, p. 299.
- (8) R. K. McDonald, *Physics Today*, June 1961, pp. 36-41.
- (9) L. J. Cutrons, E. N. Leith, C. J. Palermo, and L. J. Porcello, *IRE Transactions on Information Theory*, June 1960, pp. 386-400.

EXPLANATION OF PLATE II-1

- Fig. 1. Schematic of the interaction between a plane wave and a slit.
- Fig. 2. The action of a slit upon the space frequency, Kx , of a plane wave incident upon it.
- Fig. 3. Intensity distribution observed with an infinite aperture versus that observed with a finite aperture.

PLATE II-1

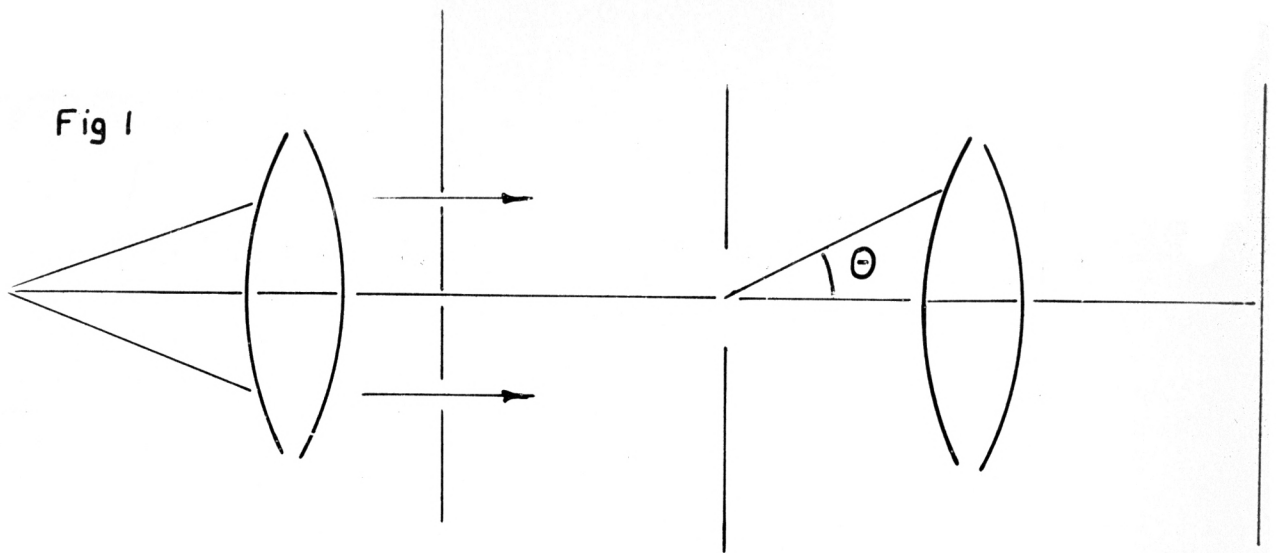


Fig 2

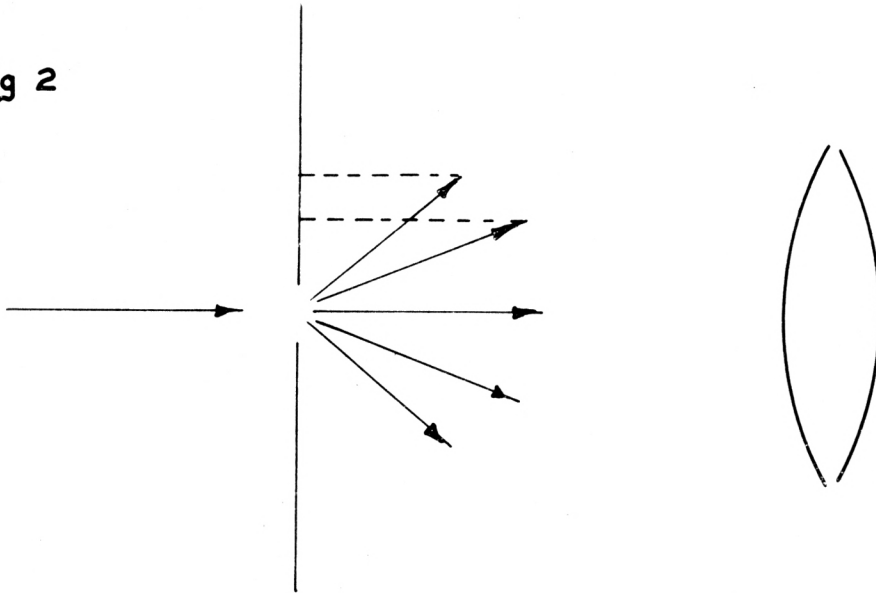
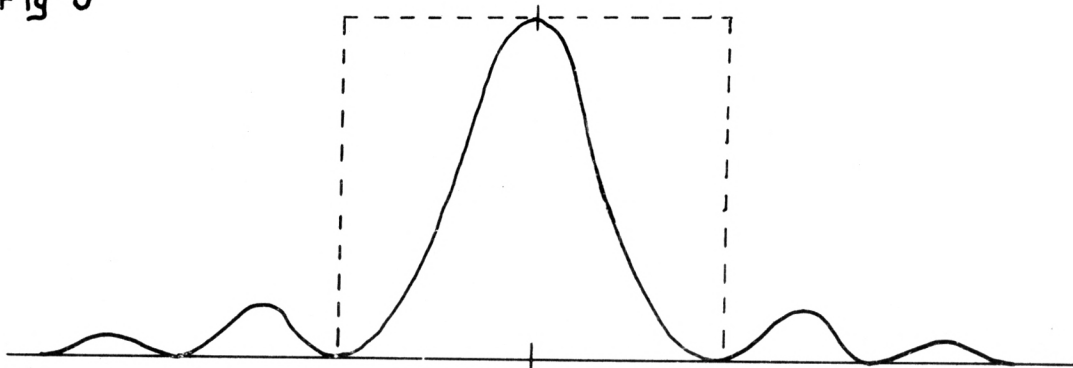


Fig 3



APPENDIX III

Phase Object Microscopy

The distribution of amplitude and phase across the primary image plane of the microscope approaches that immediately behind the object as the numerical aperture is increased, allowing more of the diffracted light to contribute to the image. The present discussion shall assume that the distribution of amplitude and phase in both the image and object planes are identical; that is, the microscope possesses perfect imagery (this tacitly implies an infinite objective aperture and an aberration free objective). Although this condition can never be rigorously attained, it provides a convenient departure point in explaining the principles of various methods of "phase object" microscopy.

Consider a completely transparent object that possesses a non-uniform optical thickness (index of refraction is a varying scalar point function); this type of object (known as a "phase object") is frequently encountered in pathology, cytology, crystallography, and other allied fields. A phase object introduces phase differences between disturbances which pass through different parts of it, but does not alter the amplitudes of these disturbances. Consequently, the disturbances immediately behind the object, and in the conjugate image plane, possess the same amplitude at all points but will show variations in phase from point to point. However, any observing instrument (the human eye included) can only distinguish changes in intensity and can not detect variations in phase so that the field of view will appear uniformly bright. Consider the vectors depicted in Figure 1 of Plate III-1. The length and directions of the thick full line vectors represent the amplitudes and phases of the disturbances at various points in the image plane of the phase object (the vectors are particular values of the complex vector field that describes

the complex disturbance over the image plane); they possess equal lengths, but have different directions. Consider that, in some manner, a disturbance of constant amplitude and phase (represented by the dotted vectors) is added to every point in the primary image plane, and that this disturbance is coherent with the existing disturbances at each point. The two disturbances will interfere with each other at each point of the image plane; and the resulting intensity (r^2) at a given point in the image plane will depend upon the phase difference between the disturbances at that point, as indicated in Figure-1. Hence, variations of optical thickness (index of refraction) in the object will cause variations in intensity in the image, which renders the phase object as an amplitude object (visible) to the detecting instrument. This technique of converting differences of phase into differences of intensity is employed in interference microscopy; and forms the basis of dark-ground and phase contrast microscopy.

The interference method (1), can be regarded in its most primitive form, as light from a source being amplitude divided into two beams, each of which traverses a separate microscope system before they are reunited. The phase object is introduced into the system traversed by one of the beams, while the other beam is left unmodulated. Upon reuniting, the two beams will interfere and the phase difference introduced into the modulated beam will cause amplitude differences in the resultant beam.

In the dark-ground method (2), (3), the same disturbance is subtracted from every point of the image; this is accomplished by either excluding the zero order light with a stop (central dark-ground illumination) or, if oblique dark-ground illumination is employed, arranging that the zero order light does not enter the microscope objective.

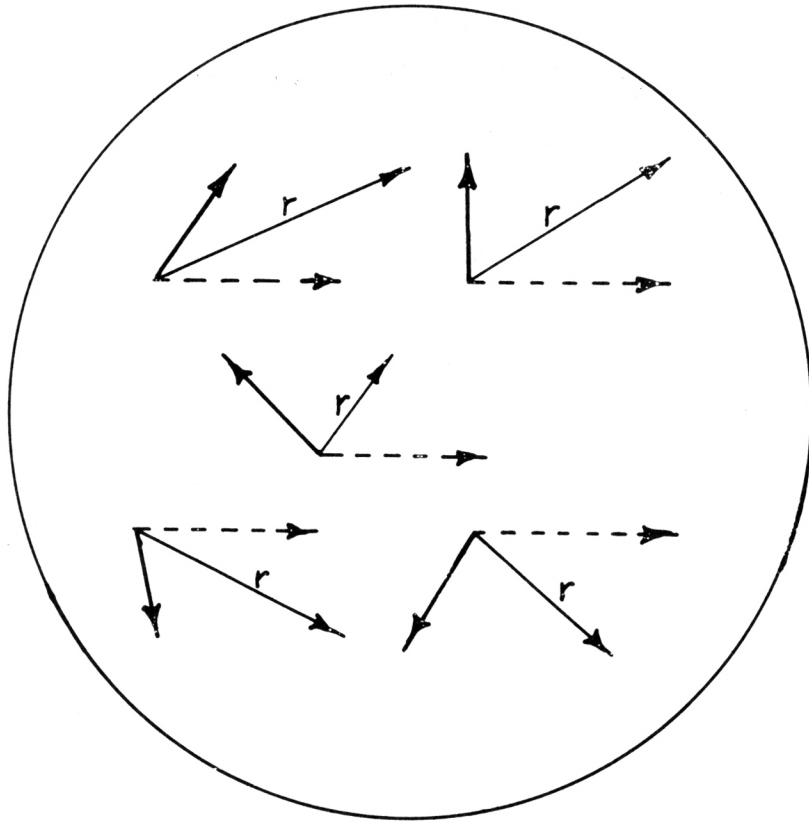
REFERENCES

- (1) J. Strong, "Concepts of Classical Optics", (1958, W. H. Freeman and Co., San Francisco), pp. 387-389.
- (2) R. S. Longhurst, "Geometrical and Physical Optics", (1957, Longmans, Green and Co., New York), pp. 298
- (3) M. Born and E. Wolf, "Principles of Optics", (1959, Pergamon Press, New York), p. 424, p. 426.

EXPLANATION OF PLATE III-1-Fig. 1.

Vector diagram of the amplitudes and phases of the disturbances at various points in the image plane of a phase object.

PLATE III-1



APPENDIX IV

Phase Contrast Microscopy

The most powerful method to date of obtaining information about "phase objects" is due to Zernike (1), and is designated as the phase contrast method. This method rests upon the modulation of light transmitted through a microscope system by the conversion of phase changes, introduced by the object, into intensity changes in the image, and possesses the distinct advantage that it produces an intensity distribution, in the image plane, which is directly proportional to the phase changes introduced by the object; that is, the intensity at any point of the image is directly proportional to the phase change due to the corresponding element of the object.

Phase contrast microscopy is a diffraction splitting technique which introduces a phase difference between the zero and higher order maxima of the Fraunhofer diffraction pattern, of the phase object, located in the back focal plane of the microscope objective. In the phase contrast method, the phase of the zero order maxima (direct light) is changed with respect to the higher order maxima (diffracted light) by introducing a disk of refracting material (phase plate) at the rear principle focus of the objective. The optical thickness, figuring, and size of this disk determines the phase delay or advance imposed upon the direct light with respect to the diffracted light.

An elementary way of portraying the process of phase contrast microscopy consists in the utilization of the series of vector diagrams depicted in Figure -1 of Plate IV-1. These vector diagrams depict the passage of the complex light disturbance through a "rudimentary" phase contrast microscope (depicted in Figure-1a) which consists of a Kohler condenser, phase object, objective, phase plate, and eyepiece.

Parallel light illuminates an "optically thin" transparent refracting object (phase object); the vectors depicted in Figure-1b represent the amplitude and phase of the parallel light illuminating the phase object. If the variations in optical thickness over the phase object are small, the light vectors, representing the complex disturbance illuminating the phase object, are rotated through small angles after passage through it. These rotations are depicted in Figure-1c; the dotted vectors representing the amplitude and phase of the light incident upon the phase object, and the full line vectors representing the amplitude and phase of the light after passage through the phase object. Let us consider the passage of just one of these light vectors passing through the phase object and follow its journey through the microscope, while examining its relationship with the light vectors missing the phase object; in that, this light vector is an arbitrarily chosen light vector, its performance passing through the microscope will certainly describe the performance of the light vectors, either singly or as a group, during their passage through the phase microscope. The rotation of this "arbitrarily chosen" light vector with respect to the light vectors missing the phase object in object space is depicted in Figure-1d. We may treat this rotated light vector as consisting of two vectors; a vector equivalent to the light vector incident upon the object (an unrotated light vector - equivalent to the light vectors missing the object) and a small difference vector. In that the optical thickness of the object is small, the difference vector will be approximately in quadrature with the unrotated light vector. This situation is depicted in Figure-1e; the full thick line vector representing the unrotated light vector and the dotted vectors representing the rotated light vector. Previously, we have utilized Abbe's theory to demonstrate that after a plane wave passes through an object, it is distributed, in object space, into an infinite number of spatial frequencies;

these spatial frequencies each, in turn, being associated with a plane wave and thus capable of being represented by a vector. Thus, we can regard the difference vector, of Figure-1e, as a sum integral over these distributed space frequency vectors, excluding the zero order frequency. Hence, the difference vector must behave as diffracted light in its passage through the microscope. Therefore, the resultant vector light field behind the object may be viewed as the superposition of a uniform vector field representing the parallel light incident upon the object plane and a "difference vector" field representing the light diffracted by the phase object. The uniform field will be converged by the objective to its rear principle focus where the phase plate resides. In traversing the phase plate, the uniform vector field will entirely pass through a region of the phase plate that will impose a uniform advance or delay upon its vectors as well as uniformly decreasing their amplitudes. Figure-1f depicts this situation; the full vector representing a wave incident upon the phase plate and the dotted vector represents a wave leaving the phase plate. After leaving the phase plate, the uniform vector field will spread out as uniform illumination over the image plane. The difference vectors spreading by diffraction across the real focal plane of the objective will largely avoid passing through that region of the phase plate that imposes an amplitude and phase change. The two vector fields recombine again in the image plane and the illumination outside the image of the object will be that due to the uniform field. However, inside the image of the object, if the uniform field has been phase delayed, the difference vectors are vectorially added to the uniform field; and if the uniform field has been phase advanced, the difference vectors are vectorially subtracted from the uniform field. Hence, retardation of the phase of the zero order maxima with respect to the diffraction spectra results in the regions of the object possessing greater optical

thickness yielding larger intensities, than the optically thinner portions of the object, in the image plane. Consequently, the object appears bright against a dark field in the eyepiece of the microscope and one speaks of bright, or negative, phase contrast. Advancement of the phase of the zero order maxima with respect to the diffraction spectra results in the regions of the object possessing greater optical thickness yielding smaller intensities than the optically thinner portions of the object, in the image plane. Consequently, the object appears dark against a bright background and one speaks of dark, or positive, phase contrast.

Phase Plate:

To comprehend the function of the phase plate, it is enlightening to note that the phase contrast method is mainly used when the variations of phase in the object are small (less than $\frac{\pi}{4}$). Also, if the phase is plotted upon an Argand diagram, it will be noted that a phase advance between 0 and $\frac{\pi}{2}$ corresponds to a phase retardation between 2π and $3\pi/2$; and that a phase retardation between 0 and $\frac{\pi}{2}$ corresponds to a phase advance between 2π and $3\pi/2$.

The typical construction of a phase microscope is depicted in Figure-2 of Plate Iv-1. A form of Kohler illumination is employed and an annular aperture (2) is placed in the back focal plane of the substage condenser. This annular aperture is conjugate to the phase plate which resides in the back focal plane of the objective.

To produce positive phase contrast, the phase plate has an annular depression (2) etched into its surface to a depth sufficient to produce a phase advance in the range $(0, \frac{\pi}{2})$ of the light passing through it with respect to the light passing through the thicker portions of the phase plate. Figure -2 depicts the path of the zero order light, illustrating that it will pass

through the thinner portion of the phase plate. Consequently, the phase of the direct light is advanced with respect to the diffracted light which passes through the thicker portions of the phase plate, yielding positive phase contrast.

If the phase plate is etched to a depth sufficient to produce a phase advance in the range of $(3\pi/2, 2\pi)$ (this is equivalent to a phase retardation in the range $(\pi/2, 0)$) of the light passing through it with respect to the light passing through the thicker portion of the phase plate, then Figure-2 illustrates that the phase of the direct light must be retarded with respect to the diffracted light, yielding negative phase contrast.

The small portion of the diffracted light that passes through the thin annulus in the phase plate results in only a slight reduction of image contrast. If t represents the depth of the depression and n is the index of refraction of the plate, the zero order is advanced in phase by $(2\pi/\lambda)(n-1)t$ with respect to most of the diffracted light. To obtain optimum performance, the phase plate must simultaneously fulfill the following requirements.

- (1) All the direct light must pass through the thin annular depression of the phase plate.
- (2) The size of the annular depression must be made as small as is consistent with requirement-1 in order to minimize the amount of diffracted light that it transmits.
- (3) The image of the annular aperture must exactly coincide with the annular depression in the phase plate.

The phase plate is made light absorbing to reduce the order of the intensity of the direct light to approximately that of the diffracted light; this increases the contrast, thus making the method more sensitive.

The simplest method of constructing a phase contrast microscope is depicted in Figure-3 of Plate IV-1. Kohler illumination is employed and the phase plate consists of a small disk, placed at the focal point of the objective, which has had a thin layer of suitable absorbing substance evaporated

upon it. Figure -3 depicts the path of the central order light, illustrating that it will pass entirely through the phase plate; where as, the diffracted light mainly misses the phase plate. Hence, the direct light is delayed in phase with respect to the diffracted light. If n is the refractive index of the substrate and d is the thickness of the layer, then the zero order light is retarded in phase by $(2\pi/\lambda)(n-1)d$ with respect to most of the diffracted spectra.

Practical realization of phase contrast is markedly affected by the size and shape of the phase advancing region on the phase plate. This phase region in turn must cover the image of the light source in order to receive all the direct light. In practical use a point source is undesirable, since it causes spurious shadows from all dust particles anywhere in the light path. To avoid these shadows, the light source should be rather broad. However, phase contrast depends on the achievement of separating the direct and diffracted light. But, the diffracted light fills the whole aperture of the objective; therefore, a part of it falls on the phase spot lessening the image contrast. Hence, the phase spot must be made as small as possible to minimize this lessening of image contrast. The best compromise of image size and shape is achieved with a long narrow shape. Commercial phase contrast microscopes employ a narrow ring shape. In order to adapt the light source to these special shapes, we use a substage condenser having in its lower focal plane an opaque disk from which the desired form is cut out. This disk acts as a secondary light source, which is imaged by the condenser and objective on the phase plate. Other methods of constructing phase plates are mentioned in references (3) and (4).

This phase contrast method of Zernike is the most sensitive available

method of making weak phase structures visible. Previously microscopists had been obliged to use the oblique illumination of dark-ground microscopy. The resulting loss of several spectra caused blurred images of the object. However, the Zernike method fully utilizes the tissue structure and renders it visible to the eye in the same manner as an ideal staining method would render it.

A very simple method of rendering visible phase objects which possess relatively large variations in thickness exists. When the phases of the direct and all the diffracted light remain unaltered under coherent illumination, the distribution of amplitude and phase in the image plane is an exact replica of that immediately behind the object. In the phase contrast method this condition is upset, and the object rendered visible, by introducing a phase difference between the direct and diffracted beams. Now, the direct and diffracted beams traverse different zones of the objective aperture. But, disturbances traversing different zones of an aperture of an optical system are out of phase in planes slightly removed from the ideal image plane (5). Therefore, a phase difference between the direct and the diffracted beams, traversing a microscope utilizing Kohler bright field illumination, can be introduced simply by slightly defocusing the microscope. This technique is sufficient to render visible variations in optical thickness which are greater than $\lambda/8$. However, this defocusing method possesses some serious shortcomings which force an observer to choose a focal position which compromises between an image which is bad because of blurring and one that is without contrast because it is too near focus (6).

Note, in all the above discussion of the use of phase object microscopes, it has been assumed that the objects are in "no" way opaque. For use with opaque objects the theory of the phase microscope must be subtly altered; however, this shall not be done here.

REFERENCES

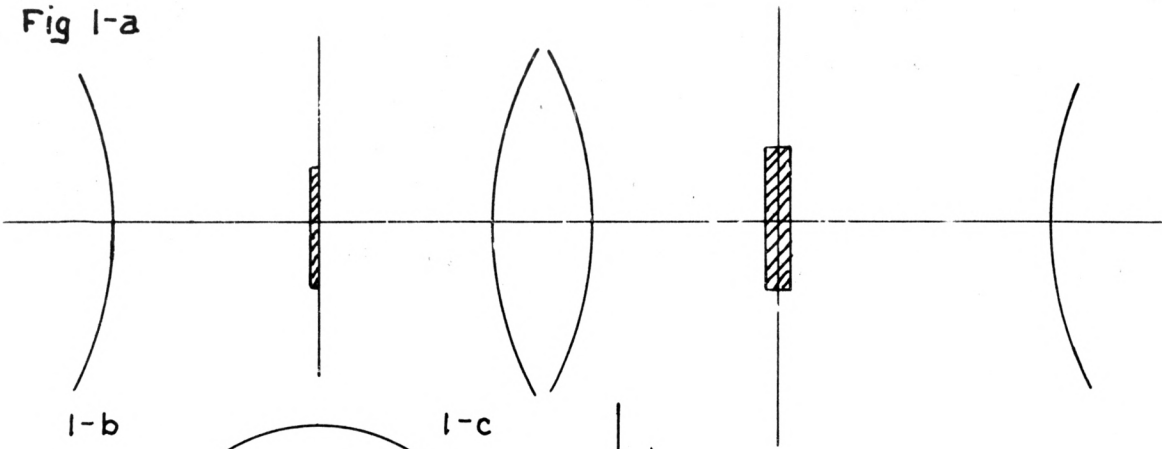
- (1) F. Zernike, Z. Tech. Phys., 16 (1935), 454; Phys. Z., 36 (1935), 848; Physica, 9 (1942), 686, 974.
- (2) J. Strong, "Concepts of Classical Optics", (1958, W. H. Freeman and Co., San Francisco), pp. 532-533.
- (3) M. Born and E. Wolf, "Principles of Optics", (1959, Pergamon Press, New York), p. 425.
- (4) A. Sommerfeld, "Optics", (1954, Academic Press, Inc., New York), p. 310
- (5) R. S. Longhurst, "Geometrical and Physical Optics", (1957, Longmans, Green and Co., New York), pp. 287-289.
- (6) J. Strong, op. cit., p. 532.

EXPLANATION OF PLATE IV-1

- Fig. 1. Vector diagrams depicting the passage of a complex light disturbance through a rudimentary phase microscope.
- Fig. 2. Typical construction of a Phase Microscope.
- Fig. 3. Simplest method of constructing a phase microscope.

PLATE IV - 1

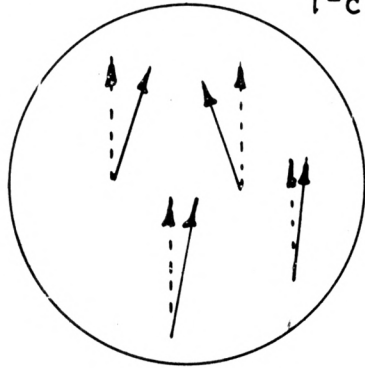
Fig 1-a



1-b



1-c



1-d



1-e



1-f



Fig 2

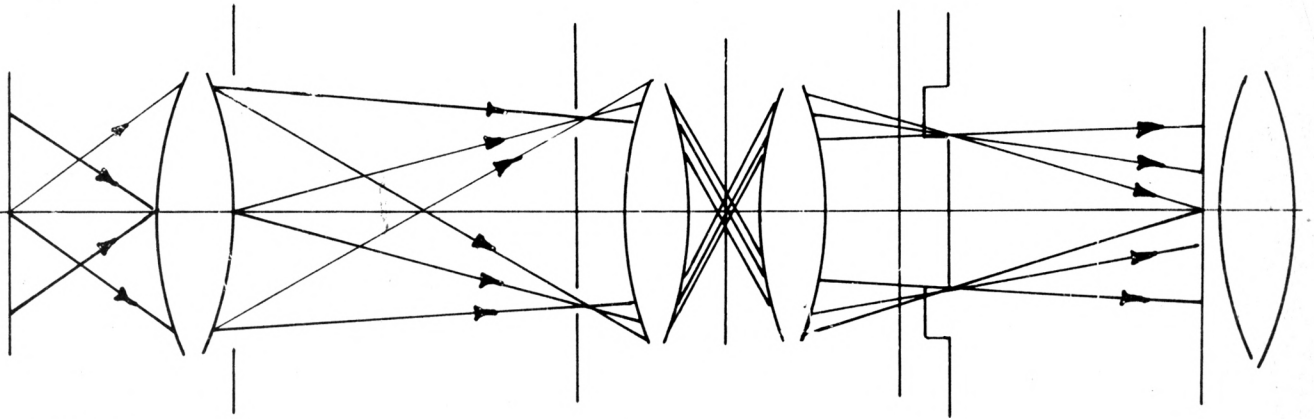
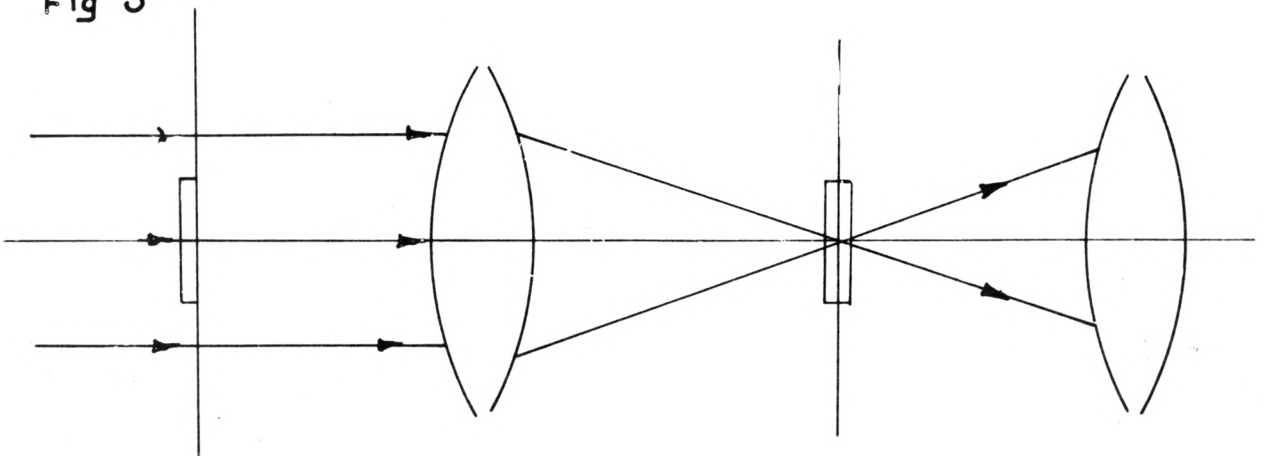


Fig 3



APPENDIX V

Mathematical Treatment of the Phase Contrast Microscope

Following the treatment of Born and Wolf (1), a mathematical analysis of the phase microscope shall be presented. Consider the schematic representation of the microscope depicted in Figure-1 of Plate V-1, illustrating the Abbe theory of image formation in a microscope when an object is illuminated by coherent illumination.

Let (x,y) be the coordinates of a typical point in the object plane where f represents the distance of the focal plane F' from the objective lens. Then Abbe's theory predicts that the disturbance $U(\xi, \eta)$ at a point

$$\xi = pf, \quad \eta = qf \quad (1)$$

when p and q are tangents of the angle between,

of the F' plane (figure-9) is given by the Fraunhofer formula

$$u(\xi, \eta) = C_1 \iint_A F(x,y) \exp \left\{ -ik \left[\frac{\xi}{f} x + \frac{\eta}{f} y \right] \right\} dx dy \quad (2)$$

where $F(x,y)$ is the transmission function of the object, C_1 is a constant, and the integration is performed over the area A of the object plane covered by the object.

In considering the transition of light from the back focal plane F' to the image plane Z' , let D' denote the distance between F' and Z' , and $V(x', y')$ be the disturbance at a typical point

$$x' = p'D', \quad y' = q'D' \quad (3)$$

of the image plane. Then, we have for Fraunhofer diffraction on the aperture in the F' plane

$$V(x', y') = C_2 \iint_B u(\xi, \eta) \exp \left\{ -ik \left[\frac{x'}{D'} \xi + \frac{y'}{D'} \eta \right] \right\} d\xi d\eta \quad (4)$$

Substituting relation (2) into relation (4) yields

$$V(x', y') = C_1 C_2 \iint_A \iint_B F(x, y) \exp \left\{ -i \frac{k}{f} \left[x + \frac{f}{D'} x' \right] \xi + \left(y + \frac{f}{D'} y' \right) \eta \right\} \frac{dx dy}{d\xi d\eta} \quad (5)$$

Defining $F(x, y)$ as zero for all points of the object plane that lie outside A permits the extension of the limits of the integration with respect to x and y to be extended over the xy -plane from $-\infty$ to $+\infty$. If the aperture B is so large that $|u(\xi, \eta)|$ is negligible for points of the F' plane that lie outside B, then the extension of the limits of the integration with respect to ξ and η may be extended over the $\xi\eta$ -plane from $-\infty$ to $+\infty$. Performing these limit extensions and noting that

$$\frac{f}{D'} = -\frac{1}{M} \quad (6)$$

where $M (< 0)$ is the magnification between Σ and Σ' , yields,

$$V(x', y') = C_1 C_2 \int_{-\infty}^{+\infty} \int_{-\infty}^{+\infty} \int_{-\infty}^{+\infty} \int_{-\infty}^{+\infty} F(x, y) \exp \left\{ -i \frac{k}{f} \left[\left(x - \frac{x'}{M} \right) \xi + \left(y - \frac{y'}{M} \right) \eta \right] \right\} dx dy d\xi d\eta \quad (7)$$

By applying the Fourier integral theorem (2) to relation (7), we obtain

$$V(x', y') = C F \left(\frac{x'}{M}, \frac{y'}{M} \right) = C F(x, y) \quad (8)$$

where (x, y) is the object point whose image is at (x', y') , $C = C_1 C_2 \lambda^2 f^2$ being a constant. Hence, provided that the aperture is sufficiently large, the image is strictly similar to the object (but inverted), both as regards the amplitude and phase.

To depict the functioning of the phase microscope in a mathematical fashion, we insert a phase plate in the back focal plane of the objective lens in Figure -1. To portray the operation of this phase plate upon the light passing through the microscope necessitates the dividing of integral (2) into two parts,

$$u(\xi, \eta) = u_0(\xi, \eta) + u_1(\xi, \eta) \quad (9)$$

where

$$u_0(\xi, \eta) = C_1 \iint_A e^{-\frac{ik}{f} \{\xi x + \eta y\}} dx dy \quad (10)$$

$$u_1(\xi, \eta) = C_1 \iint_A [F(x, y) - 1] e^{-\frac{ik}{f} \{\xi x + \eta y\}} dx dy$$

where U_0 represents the light distribution that would be obtained in the F' plane if no object were present, and U_1 represents the effect of the diffraction of light by the object. The "direct light", U_0 (corresponding to the zero order of figure-9), will be concentrated in only a small region B_0 of the F' plane, around the axial point $\xi = \eta = 0$. However, only a very small fraction of the diffracted light reaches this region B_0 ; in that, most of it is diffracted to other parts of the B -plane. Suppose that the region B_0 through which the direct light passes is just covered by the phase plate. The effect of this plate upon the direct light is described by a transmission function

$$A = a e^{id} \quad (11)$$

If the phase plate only retards or advances the phase of light which is incident upon it, then $a = 1$; however, if the phase plate also absorbs light, then $a < 1$.

Hence the light emerging from the aperture will be represented by

$$u'(\xi, \eta) = A u_0(\xi, \eta) + u_1(\xi, \eta) \quad (12)$$

Applying equation (4) to equation (12) yields, the distribution of the complex amplitude, $V(x', y')$, in the image plane as

$$V(x', y') = V_0(x', y') + V_1(x', y') \quad (13)$$

where

$$\begin{aligned} V_0(x', y') &= AC_2 \iint_B u_0(\xi, \eta) e^{-\frac{ik}{D'} [x'\xi + y'\eta]} d\xi d\eta \\ V_1(x', y') &= c_2 \iint_B u_1(\xi, \eta) e^{-\frac{ik}{D'} [x'\xi + y'\eta]} d\xi d\eta \end{aligned} \quad (14)$$

In that U_0 is practically zero outside B_0 , and since the aperture B greatly exceeds in size the region B_0 , no appreciable error is introduced by the extension of the domain of integration in V_0 over the whole F' plane. Also, assuming that B is sufficiently large enough to admit all the diffracted rays that carry any appreciable energy, allows the extension of the limits of the integral represented by V_1 over the whole F' plane without an introduction of appreciable error. Hence, assuming that the transmission function $F(x, y)$ is defined as zero at points of the object plane outside the region covered by the object, we may extend the domain of the integrals of relation (27) to be taken with infinite limits,

$$\begin{aligned} V_0 &= AC_2 \iiint_{-\infty}^{\infty} \exp \left\{ -\frac{ik}{f} \left[\xi \left(\frac{fx'}{D'} + x \right) + \eta \left(\frac{fy'}{D} + y \right) \right] \right\} d\xi d\eta \\ V_1 &= c_2 \iiint_{-\infty}^{\infty} [F(x, y) - 1] \exp \left\{ -\frac{ik}{f} \left[\xi \left(\frac{fx'}{D'} + x \right) + \eta \left(\frac{fy'}{D} + y \right) \right] \right\} d\xi d\eta \end{aligned} \quad (15)$$

Upon applying the Fourier integral theorem to relation (15) recalling relation (6), yields

$$v_0(x', y') = cA$$

$$v_1(x', y') = c \left[F\left(\frac{x'}{M}, \frac{y'}{M}\right) - 1 \right] = c \left[F(x, y) - 1 \right] \quad (16)$$

Hence from relations (16) and (13), it follows that the intensity distribution in the image plane is given by

$$I(x', y') = |v(x', y')|^2 = c^2 |A + F(x, y) - 1|^2 \quad (17)$$

If $F(x, y)$ is the transmission function of phase object, then

$$F(x, y) = e^{i\phi(x, y)} \quad (18)$$

where $\phi(x, y)$ is a real function. If we expand the exponential term of relation (18) in terms of a Maclaurin's series expansion and assume that $\phi(x, y)$ is small, then

$$F(x, y) \approx 1 + i\phi(x, y) \quad (19)$$

Thus relation (17) reduces, upon substitution of relation (18), to

$$I(x', y') = c^2 \left[a^2 + 2 \left\{ -a \cos \alpha - \omega \phi(x, y) + a \cos(\alpha - \phi(x, y)) \right\} \right] \quad (20)$$

Since $\phi(x, y)$ is assumed small, relation (20) further reduces to

$$I(x', y') = c^2 \left[a^2 + 2a\phi(x, y) \sin \alpha \right] \quad (21)$$

If the phase difference, introduced by the phase plate, represents a retardation or advance by a quarter of a period, then $\alpha = \pm \pi/2$ and relation (24) further reduces to

$$I(x', y') = c^2 \left[a^2 \pm 2a\phi(x, y) \right] \quad (22)$$

When the phase plate does not absorb any of the incident light, then $a = 1$, and

$$I(x',y') = 1 \pm 2\phi(x,y) \quad (23)$$

Thus, the intensity changes are then directly proportional to the phase variations of the object. If the plate absorbs a fraction a^2 of the incident light, then the ratio of the second term to the first term of relation (36) has the value $\pm\phi/a$; hence, the contrast is enhanced. For example, by weakening the direct light to $1/9$ of its original value, the sensitivity is increased three times.

The special case $a = 0$, corresponds to dark ground illumination and the intensity distribution will then be given by

$$I(x',y') = 2c^2 [1 - \cos\phi(x,y)] \quad (24)$$

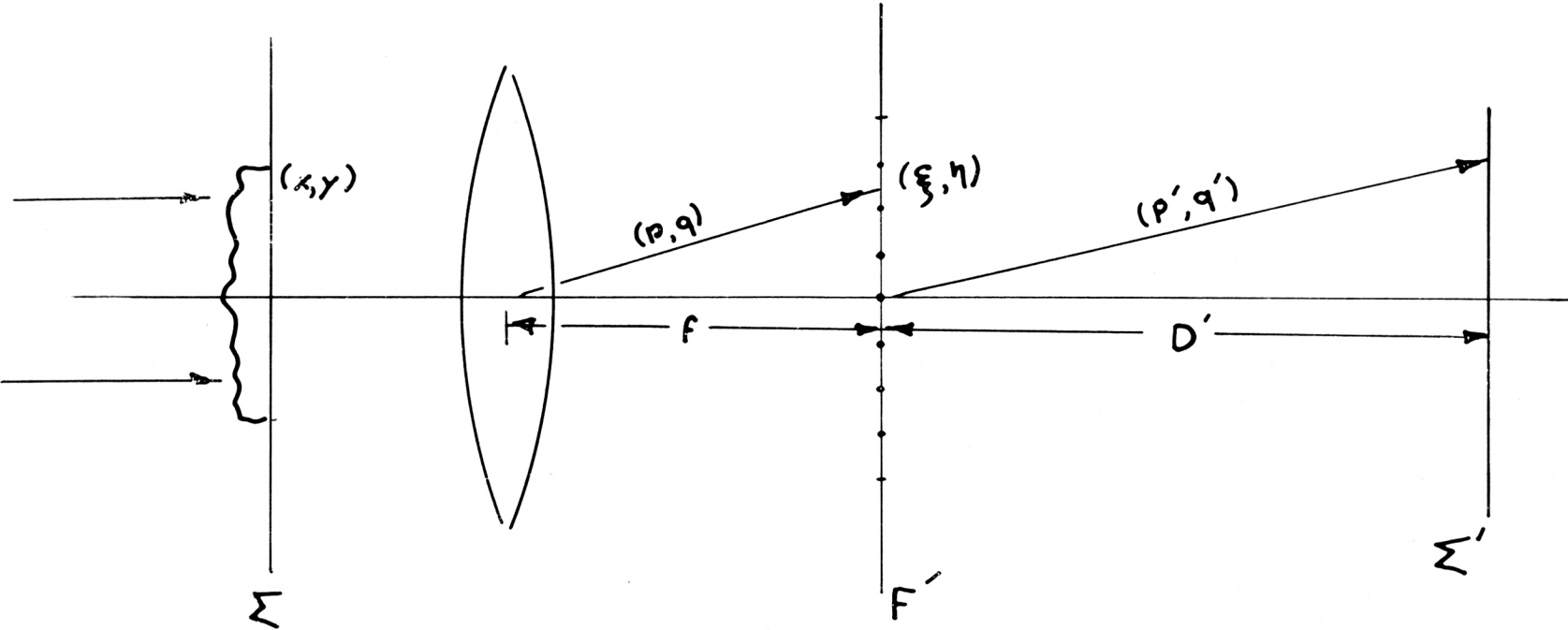
REFERENCES

- (1) M. Born and E. Wolf, "Principles of Optics", (1959, Pergamon Press, New York), p. 418 , p. 425 .
- (2) R. Courant and D. Hilbert, "Methods of Mathematical Physics", Vol. 1, p. 79.

EXPLANATION OF PLATE V-1

Schematic representation of the microscope

PLATE V-1



A STUDY OF HEAVY NUCLEAR TRACKS IN G-5 EMULSION
EMPLOYING PHASE CONTRAST PHOTOMICROGRAPHY

by

ROBERT GARY MCFADDEN

B. S., Case Institute
of Science and Technology, 1959

AN ABSTRACT OF A THESIS

submitted in partial fulfillment of the

requirements for the degree

MASTER OF SCIENCE

Department of Physics

KANSAS STATE UNIVERSITY
Manhattan, Kansas

1962

AN ABSTRACT OF A THESIS

During the fall of 1961, E. Obi and the writer, while employing a phase contrast microscope in the examination of tracks in a stack of Ilford G-5 stripped emulsions, observed that the appearance of the nuclear tracks was affected by the adjustment of the phase substage condenser. By appropriate settings of the phase condenser, the background and the granularity of the emulsion could be made to disappear, leaving only the trajectories of the very thick nuclei, stripped of most of their loose associations of delta-ray clumps. This phenomenon seemed to present a method of eliminating optically the two factors that cause the measurement of track width to be subjective; they are: (a) the loose associations of delta-rays that lie in close proximity to the track, and (b) the confusing granularities of the emulsion in the vicinity of heavy tracks. The present investigation had as its objective the development of this optical phenomenon into a systematic optical method of obtaining duplicable track width measurements of heavy nuclei, in order to employ these track width parameters in the calculation of the atomic charge Z of the investigated nuclear species.

Three photographic montages were made of a heavy nuclear track, each using a different setting of the phase condenser. Various track width measurements were performed upon these montages, but only one method proved of interest. This method consisted of obtaining a track width parameter from the planimeter tracings of the projected outlines of the track photographed under one mode of phase contrast illumination. This track width parameter proved far superior to track width parameters obtained in a similar manner under bright field illumination. Also, a relationship between the grain diameter in the Ilford G-5 emulsions used in this investigation and the track width

was observed and attributed to the manner of processing of the pellicles. The charge of the nuclear track employed in this investigation was determined as $Z = 18$ (Argon) by plotting the range at which the maximum of the experimental track width versus range curve occurred upon the theoretical curve of the atomic charge Z versus the range at which maximum track width occurs computed from Mott's delta-ray spectrum relation using Lonchamp's delta-ray criterion.

A feasible method of objectively measuring track width parameters by the use of phase contrast techniques has been delineated and this parameter may be used to compute values of the charge of heavy nuclei.